

UNSTEADY FLOW ANALYSIS OF TWO DIFFERENT ARM STROKE
TECHNIQUES IN FRONT CRAWL SWIMMING USING COMPUTATIONAL
FLUID DYNAMICS

A THESIS SUBMITTED TO
THE GRADUATE SCHOOL OF NATURAL AND APPLIED SCIENCES
OF
MIDDLE EAST TECHNICAL UNIVERSITY

BY

BİLGEHAN BOZKURT

IN PARTIAL FULFILLMENT OF THE REQUIREMENTS
FOR
THE DEGREE OF MASTER OF SCIENCE
IN
MECHANICAL ENGINEERING

DECEMBER 2021

Approval of the thesis:

**UNSTEADY FLOW ANALYSIS OF TWO DIFFERENT ARM STROKE
TECHNIQUES IN FRONT CRAWL SWIMMING USING
COMPUTATIONAL FLUID DYNAMICS**

submitted by **BİLGEHAN BOZKURT** in partial fulfillment of the requirements for
the degree of **Master of Science in Mechanical Engineering, Middle East
Technical University** by,

Prof. Dr. Halil Kalıpçılar
Dean, Graduate School of **Natural and Applied Sciences**

Prof. Dr. M. A. Sahir Arıkan
Head of the Department, **Mechanical Engineering**

Prof. Dr. Almıla Güvenç Yazıcıoğlu
Supervisor, **Mechanical Engineering, METU**

Assoc. Prof. Dr. Cüneyt Sert
Co-Supervisor, **Mechanical Engineering, METU**

Examining Committee Members:

Assist. Prof. Dr. Özgür Uğraş Baran
Mechanical Engineering Dept., METU

Prof. Dr. Almıla Güvenç Yazıcıoğlu
Mechanical Engineering Dept., METU

Assoc. Prof. Dr. Cüneyt Sert
Mechanical Engineering Dept., METU

Assist. Prof. Dr. Ali Karakuş
Mechanical Engineering Dept., METU

Assoc. Prof. Dr. Pınar Arpınar Avşar
Exercise and Sport Sciences Dept., Hacettepe University

Date: 08.12.2021

I hereby declare that all information in this document has been obtained and presented in accordance with academic rules and ethical conduct. I also declare that, as required by these rules and conduct, I have fully cited and referenced all material and results that are not original to this work.

Name Last name: Bilgehan Bozkurt

Signature: 

ABSTRACT

UNSTEADY FLOW ANALYSIS OF TWO DIFFERENT ARM STROKE TECHNIQUES IN FRONT CRAWL SWIMMING USING COMPUTATIONAL FLUID DYNAMICS

Bozkurt, Bilgehan
Master of Science, Mechanical Engineering
Supervisor: Prof. Dr. Almıla Güvenç Yazıcıoğlu
Co-Supervisor: Assoc. Prof. Dr. Cüneyt Sert

December 2021, 79 pages

This study analyzes how the propulsive force is created by the hand and arm in front crawl swimming. To answer this question, 12 swimming cases with variations in swimming velocity and arm velocity are compared using three dimensional straight and elbow angled arm models by doing unsteady flow analysis with computational fluid dynamics (CFD). The results show that the straight arm model creates more propulsive force than the angled arm. The results also reveal that linear hand velocity must be faster than swimming velocity in order to create good amount of propulsive force. In addition, the push phase of swimming has higher propulsive force than the pull phase. From this perspective, this study emphasizes the preferred arm position and the right time for a swimmer to use their effort to create the maximum propulsive force during front crawl swimming.

Keywords: Front Crawl Swimming, Propulsive Force, CFD, Unsteady Flow

ÖZ

SERBEST STİL YÜZMEDE İKİ FARKLI KOL VURUŞ TEKNİĞİNİN HESAPLAMALI AKIŞKANLAR DİNAMİĞİ İLE ZAMANA BAĞLI AKIŞ ANALİZİ

Bozkurt, Bilgehan
Yüksek Lisans, Makina Mühendisliği
Tez Yöneticisi: Prof. Dr. Almila Güvenç Yazıcıoğlu
Ortak Tez Yöneticisi: Assoc. Prof. Dr. Cüneyt Sert

Aralık 2021, 79 sayfa

Bu çalışma, serbest stil yüzmede el ve kol tarafından oluşturulan itki kuvvetinin nasıl oluştuğunu analiz etmektedir. Bu soruyu yanıtlamak için, yüzme hızı ve kol hızının farklı birleşimleriyle oluşturulan 12 yüzme vakası, üç boyutlu düz kol ve dirsek açılı kol modellerini kullanarak, hesaplamalı akışkanlar dinamiği (HAD) ile zamana bağlı akış analizi yapılarak karşılaştırılmıştır. Sonuçlar, düz kolun açılı koldan daha fazla itki kuvveti oluşturduğunu göstermektedir. Sonuçlar ayrıca, yüksek miktarda itki kuvveti oluşturmak için el hızının yüzme hızından daha fazla olması gerektiğini ortaya koymaktadır. Ayrıca yüzmenin itme fazının, çekme fazından daha yüksek itki kuvvetine sahip olduğu belirlenmiştir. Bu bakış açısıyla, bu çalışma, yüzücülerin serbest stil yüzme sırasında maksimum itki kuvveti oluşturacak eforu harcamaları için doğru zamanı ve doğru kol pozisyonunu vurgulamaktadır.

Anahtar Kelimeler: Serbest Stil Yüzme, İtki Kuvveti, HAD, Zamana Bağlı Akış

To my sweetheart

ACKNOWLEDGMENTS

I would like to thank and express my deep and sincere gratitude to my thesis advisor Prof. Dr. Almıla Güvenç Yazıcıođlu for her guidance, support, and encouragement and to my co-supervisor Assoc. Dr. Cüneyt Sert for his valuable contribution and guidance.

I would like to thank the jury members of my thesis, Assoc. Prof. Dr. Pınar Arpınar Avşar, Assist. Prof. Dr. Özgür Uğraş Baran, and Assist. Prof. Dr. Ali Karakuş for their constructive contribution to the swimming model and CFD analysis of this thesis.

I would like to thank my family, my father Necati Bozkurt, my mother Gülay Bozkurt, and my sister Burcu Bozkurt for their support throughout my life.

Last but not least, I would like to thank my beautiful girlfriend Elif Yıldırım who has given an amazing support and endless patience throughout my graduate education and in writing my thesis. She is the one who makes my life meaningful, peaceful, and enjoyable. I feel so lucky to have her.

TABLE OF CONTENTS

ABSTRACT	v
ÖZ	vi
ACKNOWLEDGMENTS	viii
TABLE OF CONTENTS	ix
LIST OF TABLES	xi
LIST OF FIGURES	xii
LIST OF ABBREVIATIONS	xv
LIST OF SYMBOLS	xvi
1 INTRODUCTION	1
1.1 Swimming Disciplines	4
1.1.1 Front Crawl Swimming	7
1.2 Orientation of the Hand/Arm.....	13
1.3 Outline of the Thesis	15
2 LITERATURE REVIEW.....	17
2.1 Computational and Experimental Studies	17
2.2 Steady vs Unsteady Simulations.....	26
2.3 Turbulence Modelling	29
2.4 Summary of the Literature.....	31
3 CFD MODEL	37
3.1 Geometry Creation.....	37
3.2 Solution Domain and Boundary Conditions.....	40
3.2.1 Investigated Cases and Boundary Conditions.....	42

3.3	Mesh Generation and Mesh Independence Study.....	46
3.3.1	Mesh Independence Study	51
3.3.2	Sliding Mesh Technique	53
3.4	CFD Setup	54
4	RESULTS.....	57
4.1	Propulsive Force Results	57
4.2	Pressure Results	62
4.3	Velocity Results	67
5	CONCLUSION.....	71
5.1	Summary of the Study.....	71
5.2	Major Conclusions	72
5.3	Future Work.....	72
	REFERENCES	75

LIST OF TABLES

TABLES

Table 1.1 A simple comparison between CFD and experimental methods [8].....	4
Table 2.1 CFD research related to front crawl swimming.....	33
Table 2.2 Experimental studies on human swimming.....	35
Table 3.1 Investigated swimming cases in this study.....	43
Table 3.2 Boundary conditions' details	45
Table 3.3 Details of the inflation (boundary layer) mesh	49
Table 3.4 Mesh independence study parameters. Mesh-4 is selected for the CFD analysis.....	52
Table 3.5 CFD setup parameters	55
Table 4.1 Observed maximum instantaneous propulsive force values and corresponding arm position in terms of sweepback angle.	61
Table 4.2 Mean propulsive force during pull and push phases	62

LIST OF FIGURES

FIGURES

Figure 1.1. A cyclist needs to overcome forces of air resistance in order to move forward [1].	2
Figure 1.2 Schematic overview of the forces acting on the entire swimmer and the swimmer's hand. The propulsive force can be generated by hand/arm. [3]	3
Figure 1.3 Breaststroke technique stages [9]	5
Figure 1.4 Butterfly swimming technique [9]	6
Figure 1.5 Illustration of the backstroke technique of an Olympic swimmer, Aaron Peirsol. [9]	7
Figure 1.6 The "streamline position" during glide before starting arm stroke, as viewed from the bottom of the pool. The legs are extended just like the arms. [10]	8
Figure 1.7 Stroke phases in front crawl swimming. [9]	9
Figure 1.8 Body rotation for breathing during front crawl swimming. [10]	10
Figure 1.9 Phases of the front crawl swimming arm stroke [11]	11
Figure 1.10. Forces acting on the hand during swimming, at an arbitrary position in an instantaneous time during the pull phase. [15]	13
Figure 1.11 Sweepback angle	14
Figure 1.12 Angle of attack	14
Figure 1.13 Yaw angle	15
Figure 2.1 Test apparatus of Sidelnik and Young [16]	19
Figure 2.2 Test apparatus of Takagi et al. [17]	20
Figure 2.3 Vorticity distribution (left) and velocity distribution (right) of Takagi et al. [17]. There is a 67 ms time difference between the top and bottom instances. At the moment in the top figure, shedding vortex occurs due to the motion in the x-direction. At the moment in the bottom figure, in addition to the shedding vortex, a bound vortex occurs when a movement in z-direction occurs in addition to x-direction movement.	21
Figure 2.4 Video cameras and the human subject in Gourgulis et al. [19]	22

Figure 2.5 Variation of drag coefficients with angle of attack in Schleihau [2] and Bilinauskaite et al. [20]. Bilinauskaite et al. [23] uses appropriate velocity and sweepback angle values in order to compare their study with Bixler and Riewald [12] and Schleihau [2]	24
Figure 2.6 Two vortices lead to the drag force for Takagi et al. [17] and Samson et al. [21]. Red color indicates counter-clockwise vortices and blue is for clockwise [17].....	25
Figure 2.7 Arm strokes can create flow mixing and swirling during front crawl swimming	30
Figure 3.1 Different views of the straight arm model. (a) Parts of the straight arm model (b) Top view of the straight arm model. (x-z plane) (c) Front view of the model. (x-y plane) (d) Close view to the shoulder of the straight arm model (z-y plane) (e) Close view to the tip of the hand of the straight arm model	38
Figure 3.2 145° elbow angle is observed in Michael Phelps' front crawl swimming technique	39
Figure 3.3 Elbow angle is created between the forearm and the upper arm.....	39
Figure 3.4 Elbow angle is 145°.....	40
Figure 3.5 Cylinder region which has the hand/arm model in itself, is located inside the box region.....	41
Figure 3.6 Hand/arm model location inside the solution domain	41
Figure 3.7 Solution domain measurements. L is the total arm length which is nearly 80 cm.....	42
Figure 3.8 Boundary conditions	44
Figure 3.9 Mesh structure of the solution domain.....	46
Figure 3.10 Cylinder body mesh structure.....	47
Figure 3.11 y+ values on the arm at different times	48
Figure 3.12 Inflation layer close to the shoulder.....	49
Figure 3.13 Inflation layer close to the tip of the hand.....	50
Figure 3.14 Mesh structure on hand segment	51
Figure 3.15 Force result in -x direction of the mesh independence study	53

Figure 3.16 Sliding mesh technique for this study	54
Figure 4.1 Propulsive force values for different swimming cases at different sweepback angle	58
Figure 4.2 Mean Pressure Differences between Anterior and Posterior part of the Hand/Arm.....	63
Figure 4.3 High and low pressure regions around 1 m/s & 6.28 rad/s case of the straight and angled arm models at different sweepback angles in x-y plane (z=0). Red zone shows the pressure higher than 1014 Pa; blue zone indicates the pressure is lower than -3420 Pa.....	66
Figure 4.4 Relative velocity (with respect to the cylinder body) contour of the swimming case that has highest propulsive force. Contour on the left belongs to 1B which is highest propulsive force observed case and, on the right, belongs to 2E, which is the lowest. Sweepback angle values of the hand/arm positions are located on the right-lower side of the each hand/arm model.	69

LIST OF ABBREVIATIONS

ABBREVIATIONS

CFD	Computational Fluid Dynamics
SST	Shear Stress Transport
PIV	Particle Image Velocimetry

LIST OF SYMBOLS

SYMBOLS

\vec{D}	Drag Force, N
\vec{F}_n	Normal Force, N
\vec{F}_t	Tangential Force, N
\vec{L}	Lift Force, N

CHAPTER 1

INTRODUCTION

Athletes in different sports disciplines attempt to increase their performance of sport-specific skills through the help of scientific research, which involves the fields of physics, biomechanics, engineering, and many more. Spending as little energy and time as possible while moving forward in a competition is crucial for sports, such as athletics, marathon running, cycling, and swimming. The physical environment of the sport and its effect on the athlete are very important factors on the athlete's movement efficiency, especially in sports such as cycling and swimming, which respectively involve gas and liquid environments. For instance, in cycling, cyclists use their energy in order to move through air, so that they overcome air resistance while moving forward. Some of the forces acting on a cyclist are shown in Fig 1.1, where it is observed that a cyclist needs to create some forces in order to cope with air and road resistance. The fluid environment has a negative effect on moving forward for both cyclists and swimmers. However, the cyclist pedals in order to generate propulsive forces by using the bicycle mechanism, which does not involve using air (the fluid environment) to create pushing forces.

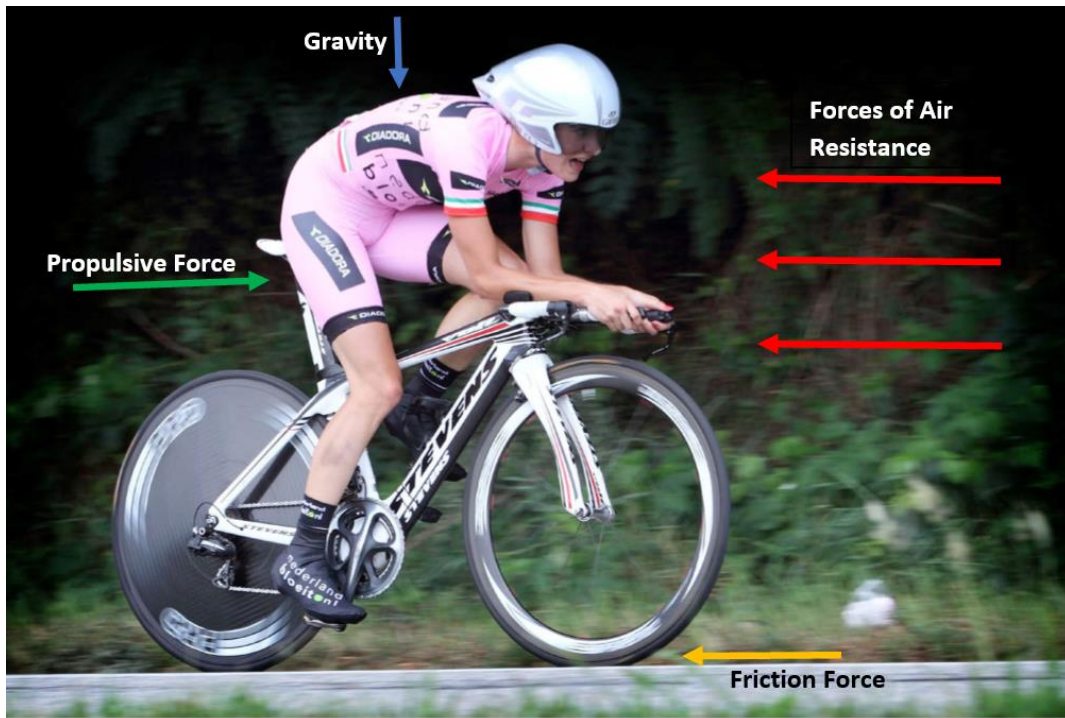


Figure 1.1. A cyclist needs to overcome forces of air resistance in order to move forward [1]

On the other hand, swimmers must use their fluid environment by directly utilizing their body segments in order to move forward. Furthermore, cycling and swimming have similar force configurations, except buoyancy force, which is not a directly relevant force for a swimmer in order to move forward (see Fig 1.2). Therefore, the body movements swimmers perform in creating propulsive force to move forward in the water need to be identified. These are arm pulls and leg strikes that a swimmer does using the fluid they are swimming in. As Figure 1.2. shows, arm pulling for this type of swimming can create propulsion in order to overcome drag. Detailed information about drag will be further elaborated in Section 1.1.1.1.

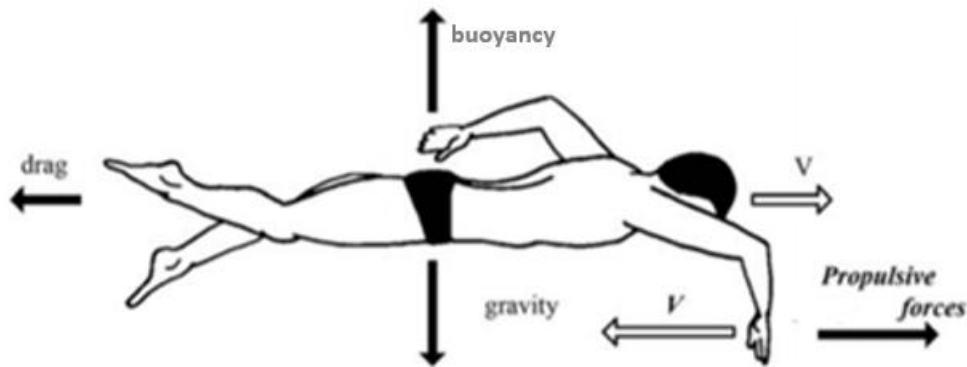


Figure 1.2 Schematic overview of the forces acting on the entire swimmer and the swimmer's hand. The propulsive force can be generated by hand/arm. [3]

In sum, it can be deduced that in any other sport except water sports such as swimming, water polo, synchronized swimming etc., this kind of dependency on the fluid environment is usually not observed. Therefore, experimental studies on swimming have mostly focused on the interaction of swimmers with the surrounding fluid environment. Experiments by using water channels [2], [3], towing tanks [4]; [5], and wind tunnels [6]; [7] are some techniques to understand the fluid's impact on the swimmer. These types of experiments have created new approaches to better study the swimming mechanism. With technological developments, other methods to analyze swimming have emerged and started assisting experimental studies. Computational Fluid Dynamics (CFD) is one of these techniques, which can help create relatively simple models in order to overcome the complexity that arises from dynamic body motion in swimming and the movement of water, but still provide realistic solutions while saving time. This issue will be further discussed in detail in Chapter 2.

In Table 1.1 a rough comparison of CFD and experimental methods is provided. CFD analyses are generally cheaper, quicker, safer, repeatable, can use different scales of a model, and can give information not only on the measured points in a model, but on the whole model. However, CFD solutions are approximate by nature and

accurately predicting the errors involved can sometimes be difficult. It is possible that a seemingly logical CFD solution can be numerically incorrect. Therefore, it is still important to validate CFD solutions with theoretical or experimental data.

Table 1.1 A simple comparison between CFD and experimental methods [8].

	CFD	EXPERIMENT
Cost	Cheaper	More expensive
Time	Shorter	Longer
Scale	Any scale can be modeled	Small/Medium
Information	All of the domain	Measured points only
Repeatability	Yes	Only to some extent
Security	Safe	Some risk is involved

1.1 Swimming Disciplines

Swimming stroke includes repeated body movements in order to move further in water with less effort. Breathing during swimming is in harmony with these movements. There are currently plenty of motions in order to propel a body to move forward or for other purposes¹. Swimmers train and race in a pool in four swimming disciplines: breaststroke, butterfly, backstroke, and the technique that is the topic of this thesis, front crawl, which is the predominantly used stroke during training.

In breaststroke technique (see Fig 1.3), swimmers lay down on their chest and keep prone position without body rotation. Arm/hand and leg movements are left-right

¹ Some of the swimming styles other than the four most common styles of backstroke, breaststroke, butterfly, and front crawl swimming are the following.

Dog Paddle: In this stroke, swimmers lay down on their chest and they move their legs and arms alternately in a manner reminding like a dog's swim.

Treading water: This is one of the swimming styles whose purpose is not to propel the body to move forward, but rather to stay upright and floating. For example, in some of the swimming sports such as water polo, it is important to hold the head outside of the water for long times. For this purpose, swimmers move their legs and arms in the vertical direction with different techniques. Eggbeater kick is an example. See: "Training – Double Med-Ball Eggbeater" 2020. GoSwim TV. Accessed November 10. <https://blog.goswim.tv/articles/5430>.

symmetrical. Breaststroke technique is slower than the other swimming disciplines. However, breaststroke technique enables a comfortable swimming in slow speeds, since the head goes further outside the water during the breathing stage.

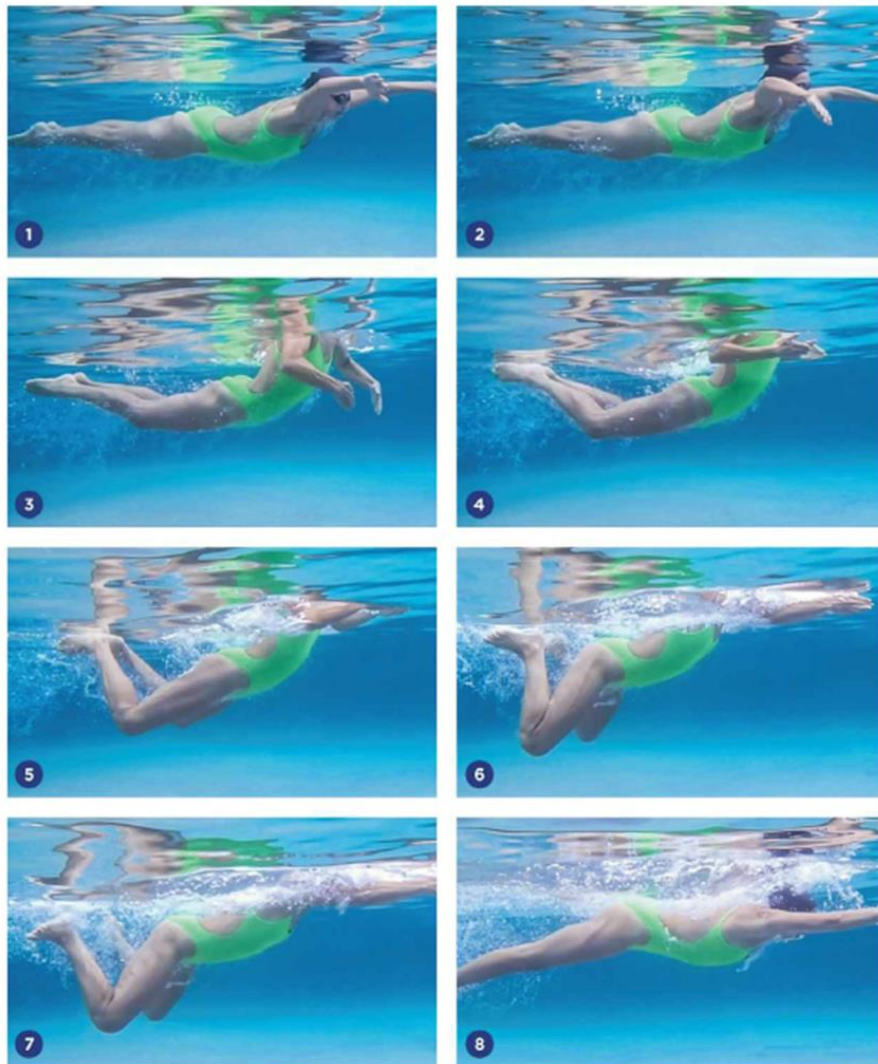


Figure 1.3 Breaststroke technique stages [9]

Butterfly technique (see Fig 1.4) is swum on the chest like the breaststroke technique. The arms move in a symmetrical movement, whereas the legs do a movement which is called “dolphin kick”. Butterfly stroke requires a relatively good understanding of its technique and strong muscles compared to other swimming disciplines. For this

reason, butterfly style is not recommended for people who are just starting to swim. It is a newer style than others².

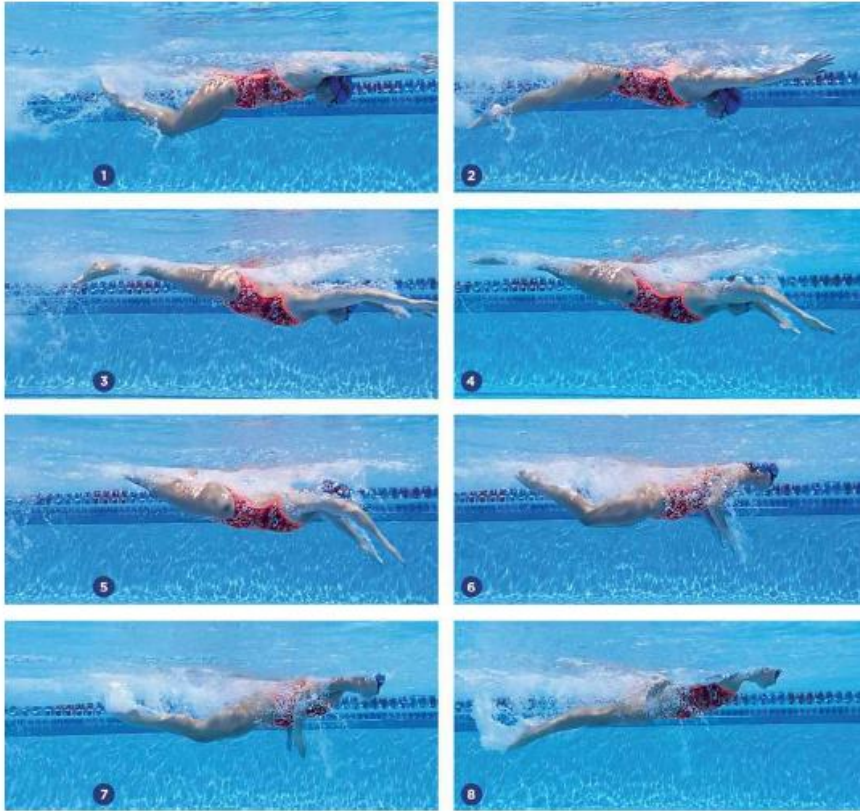


Figure 1.4 Butterfly swimming technique [9]

The backstroke technique requires swimming in a supine position unlike the other disciplines. It can be thought of as the upside down of front crawl swimming. While providing an easier breathing opportunity as an advantage, swimmers cannot see in which direction they are moving, therefore they need a smoother technique in order to go forward more efficiently. In Figure 1.5, snapshots of the backstroke technique of Aaron Peirsol, an Olympic swimmer, can be seen.

² It was first started in 1933 by adapting the breaststroke style. (Source: <https://www.newyorker.com/sports/sporting-scene/the-murky-history-of-the-butterfly-stroke>)

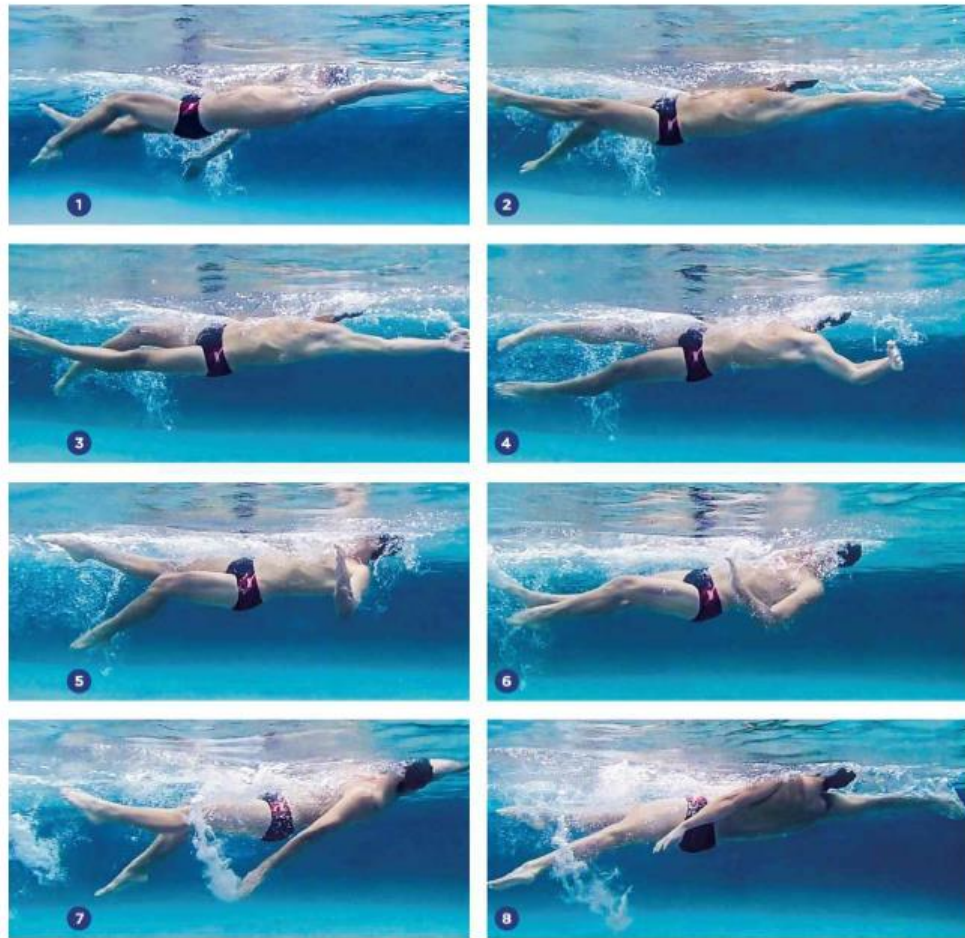


Figure 1.5 Illustration of the backstroke technique of an Olympic swimmer, Aaron Peirsol. [9]

1.1.1 Front Crawl Swimming

As it can be seen in Fig 1.6, swimming in front-crawl style starts in the streamline position, with the hands pointing towards the swimming direction and the legs in the opposite direction. After the initial phase, the arms start their movements alternately. Generally, one arm pulls the water towards the hips while the other arm in front rests on the surface of the water. Then the arm that is resting enters the water and begins the pulling process. Each completed arm movement, called a stroke cycle, is shown in Fig 1.7. For different swimming purposes, stroke rate, depth, and length in these

stroke cycles may differ. For example, it becomes important to swim with energy conservation while swimming in a pool or open water for long distances. Especially during long distance open water swimming, as the swimmer may be exposed to more drag force due to the waves, he attempts to reduce the drag force rather than creating a propulsive force, since he needs to reserve his energy for long periods. The swimmer tries to reduce the current drag force and avoid creating extra drag force by opting for softer arm strokes and fewer foot strokes.

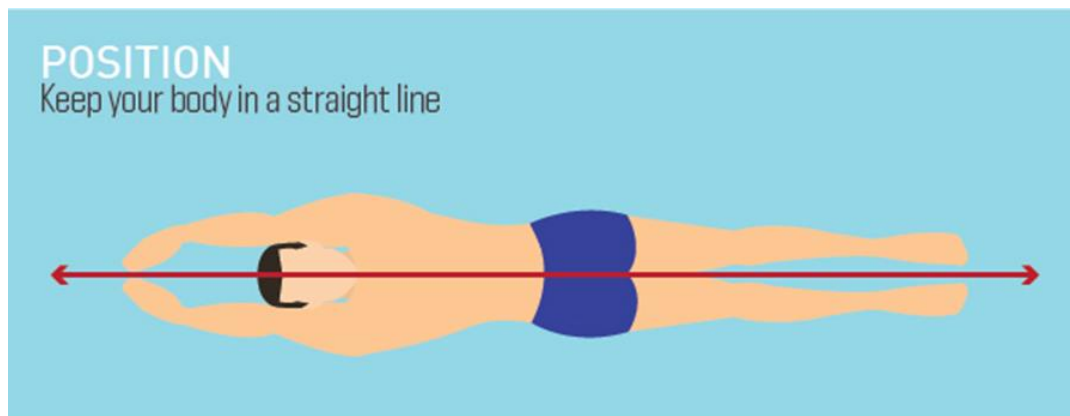


Figure 1.6 The “streamline position” during glide before starting arm stroke, as viewed from the bottom of the pool. The legs are extended just like the arms. [10]

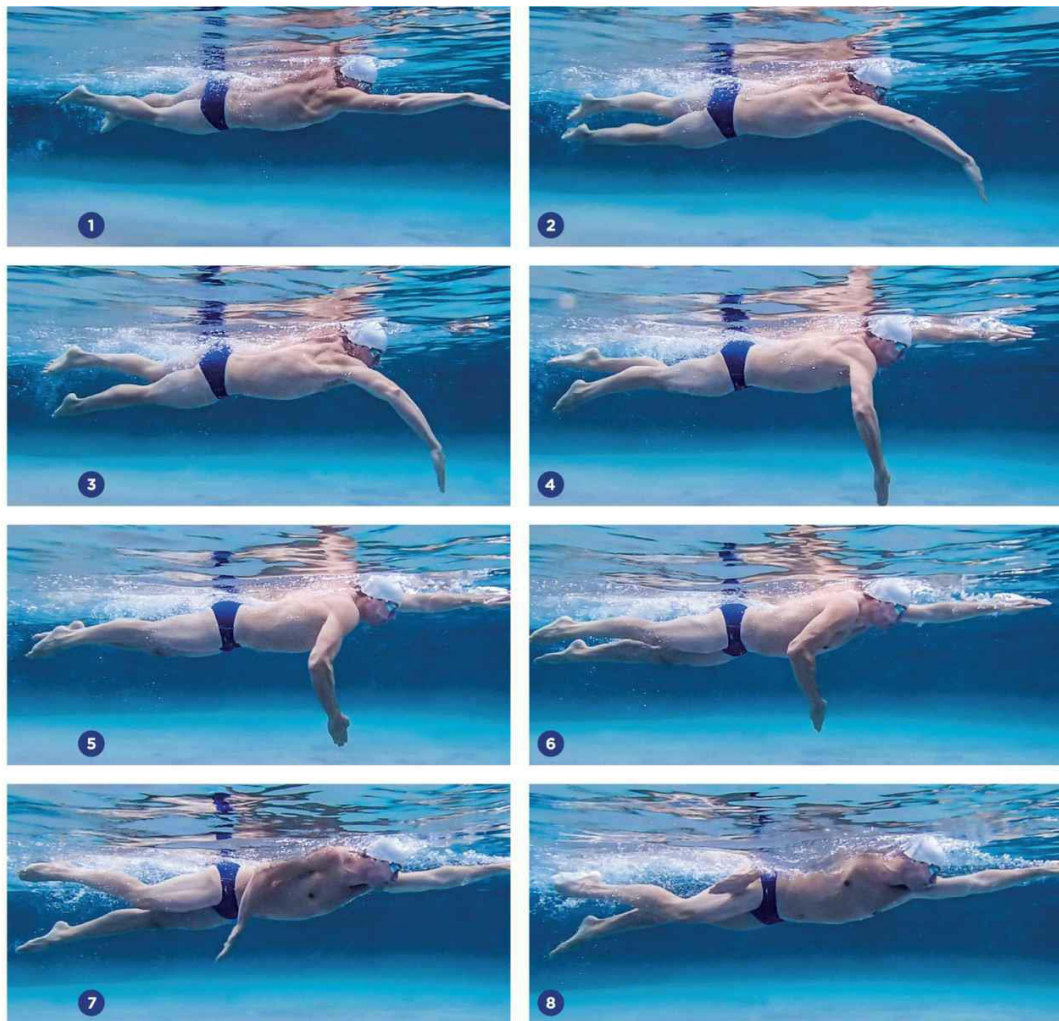


Figure 1.7 Stroke phases in front crawl swimming. [9]

During front crawl swimming, many parts of the body actively or passively affect swimming performance in some way. Head, torso, hands, arms, and legs all impact front crawl swimming. For instance, in order to minimize the drag force originating from the head, swimming instructors recommend looking at the bottom of the water at a 45° angle. As it can be observed in Fig 1.8, after a stroke cycle is over, the body rotates $30\text{-}40^\circ$ around an axis so that the head remains fixed: part of the face comes out of the water, the swimmer breathes, and then the other stroke cycle starts by breathing out through the nose and/or mouth in the water. Thus, the swimmer avoids the formation of extra drag force by trying to maintain the streamlined position during breathing.

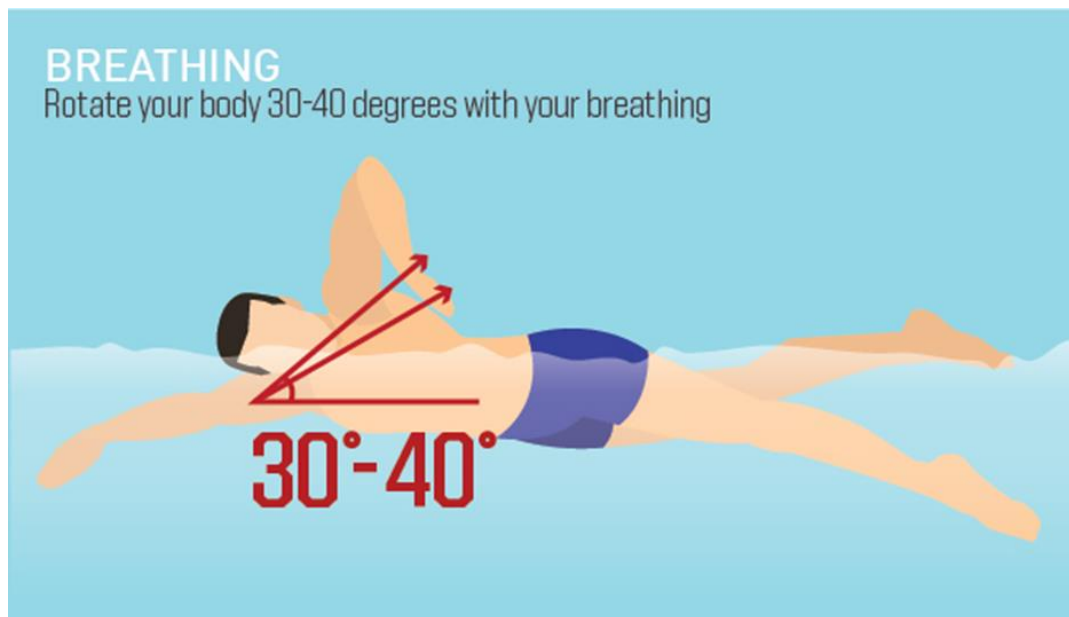


Figure 1.8 Body rotation for breathing during front crawl swimming. [10]

While swimming, the feet are used to stabilize the body position, as they contribute little to the overall speed, especially in long distances. Often during front crawl swimming, a foot kick called a flutter kick is used. In flutter kick, the legs move alternately, with one leg kicking downward while the other leg moves upward. Consequently, the perpendicular drag force acting on the body is reduced. With the body parts mentioned above, it is aimed to reduce the drag force acting on the body in general. However, creating the propulsive force is just as important as reducing the drag force, in forward motion. At this stage, the water is caught and pushed towards the hips by the movement of the hands and arms. With this movement, the normal force acting on the arms is used positively by the swimmer to move through the water. To better understand these arm movements, sports scientists have studied front crawl swimming in four stages. These are entry/catch, pull, push, and recovery, as seen in Fig 1.9 (from number 1 to number 6). In the catch phase (1-2 in Fig 1.9), while one arm is about to enter the recovery phase, the other arm enters the water and tries to catch as much water as possible. In the pull phase (2-3 in Fig 1.9), the caught water is begun to be pulled. When the arm becomes perpendicular to the water surface, the push phase (3-4 in Fig 1.9) begins, and the water is pushed towards the

hips. Finally, the arm passes to the recovery phase (4-5) out of the water and the catch phase starts for the other arm.

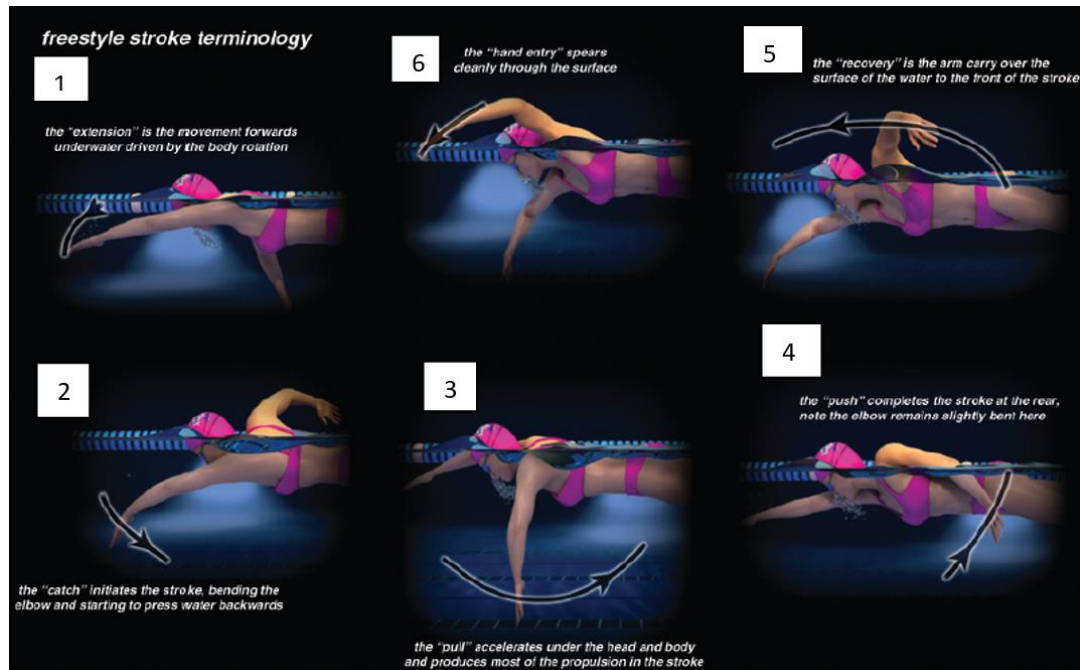


Figure 1.9 Phases of the front crawl swimming arm stroke [11]

1.1.1.1 Forces in Front Crawl Swimming

In front crawl swimming, there are different types of motion. Basically, a swimmer has rotational arm motion and translational motion to move forward. These two types of motion in a fluid result in some hydrodynamic forces during swimming. In all of the front crawl swimming stages, the arm is subjected to certain forces due to having hand/arm motion inside a dense fluid, water, and by using these forces (producing forces equal to or greater than these forces with body energy), the swimmer enables herself/himself to move through the water.

However, due to having translational motion inside water, swimmers are exerted drag force that makes them slow down. Although drag force cannot directly be used to create propulsive force, keeping a more streamlined position during translational motion may reduce the negative effects of this drag force. Velocity vectors and force

components can be seen in Figure 1.10. Two hand figures for an instantaneous time during swimming are used to show velocity vectors and force components. The hand figure on the left-hand side has velocity vectors around itself. For an instantaneous time during swimming, there are two velocity vectors: Swimming velocity (\vec{V}_s) which indicates the swimmers' motion in the forward direction and rotational velocity of the hand/arm segment ($\vec{\omega}_h$) which expresses rotational motion of the hand/arm during swimming. Velocity vector on the fingertip (\vec{V}_h) indicates the rotational velocity component of the rotational velocity of the hand/arm segment. These two translational and rotational motions during swimming results in two different reaction forces. On the right-hand side, in Fig. 1.10, force components of the two reaction forces are shown. One of the reaction forces acting on the hand/arm segment comes from the motion in the swimming direction. This reaction force has two force components: Drag force (\vec{D}), which is in an opposite direction to the swimming velocity (\vec{V}_s) and lift force (\vec{L}), which is perpendicular to the (\vec{D}). In addition to this reaction force, another reaction force occurs due to the rotational motion of the hand/arm segment. Normal force (\vec{F}_n), which is in an opposite direction to the \vec{V}_h for each instantaneous time and rotational lift force (\vec{F}_t), which is perpendicular to the \vec{F}_n , are the two force components of another reaction force.

In Fig. 1.10, the horizontal axis is the x-axis and vertical axis is the y-axis. Thus, forward direction in swimming is selected as the negative x-axis direction. In order to find the propulsive force from the reaction forces, force components on the negative x-axis direction need to be investigated. The angle between the negative x-axis and (\vec{D}) is 180° , (\vec{L}) is 90° , (\vec{F}_n) is α and (\vec{F}_t) is β . Therefore, propulsive force (\vec{F}_p) becomes the following:

$$\vec{F}_p = \vec{D}. \cos(180^\circ) + \vec{L}. \cos(90^\circ) + \vec{F}_n. \cos(\alpha) + \vec{F}_t. \cos(\beta)$$

$$\vec{F}_p = \vec{F}_n. \cos(\alpha) + \vec{F}_t. \cos(\beta) - \vec{D}$$

Thus, propulsive force depends on normal force, tangential force and drag force.

The effect and contribution of both reaction forces on the propulsive force has been studied by many researchers ([12]; [13]; [14]). This thesis examines the forces acting on the hand/arm at different arm stages during front crawl swimming using CFD.

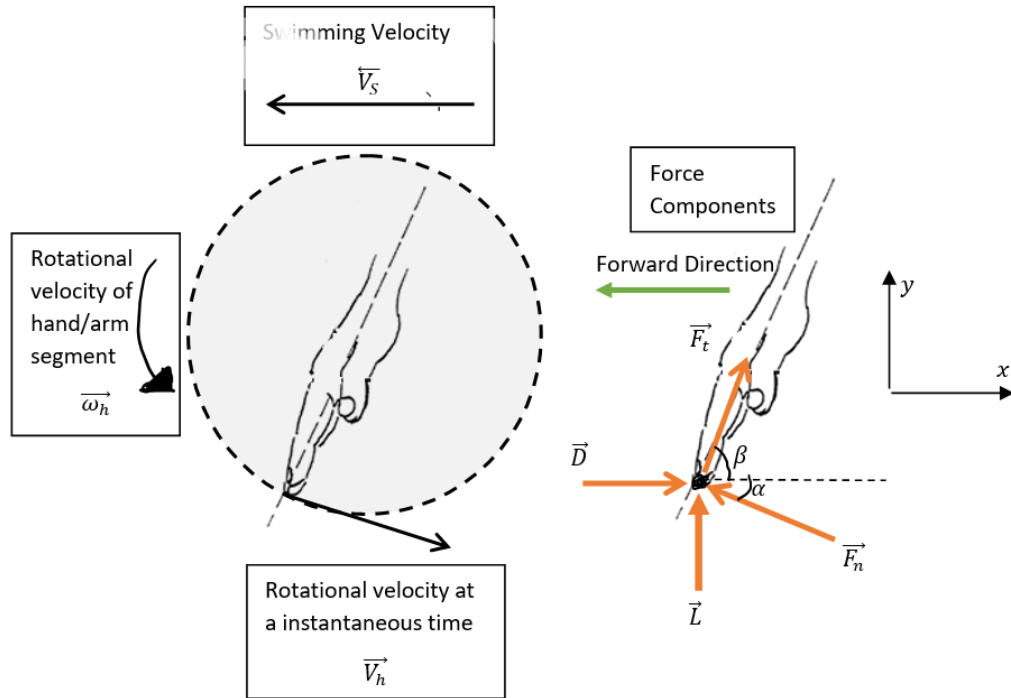


Figure 1.10. Forces acting on the hand during swimming, at an arbitrary position in an instantaneous time during the pull phase. [15]

1.2 Orientation of the Hand/Arm

In front crawl swimming, the orientation of the hand/arm is defined with three angles: Sweepback angle, angle of attack, and yaw angle. In literature, different definitions and names may be seen for these angles. For this research, sweepback angle is defined as the angle between the negative x-axis and the longitudinal axis of the hand/arm model in the x-y plane (Fig 1.11). Angle of attack is the angle between the z-axis and the lateral axis of the hand in the y-z plane (Fig 1.12). Yaw angle is the angle between the negative x-axis and the longitudinal axis of the hand/arm in the x-z plane (Fig 1.13)

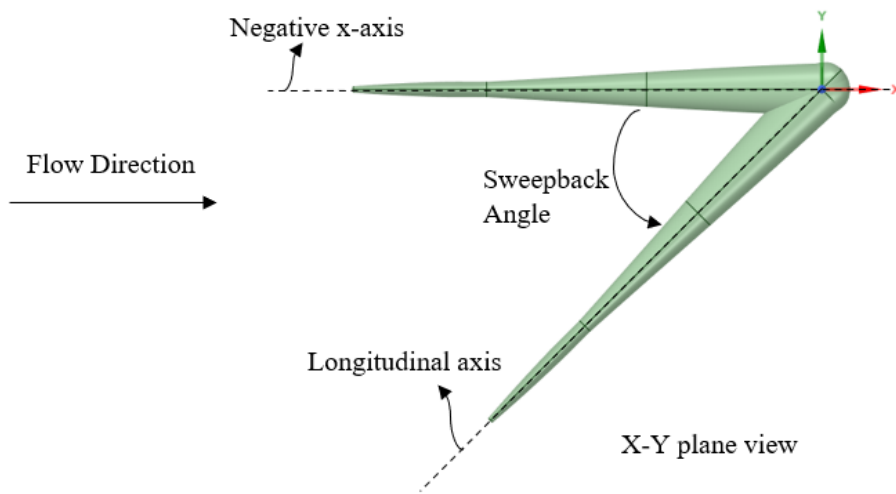


Figure 1.11 Sweepback angle

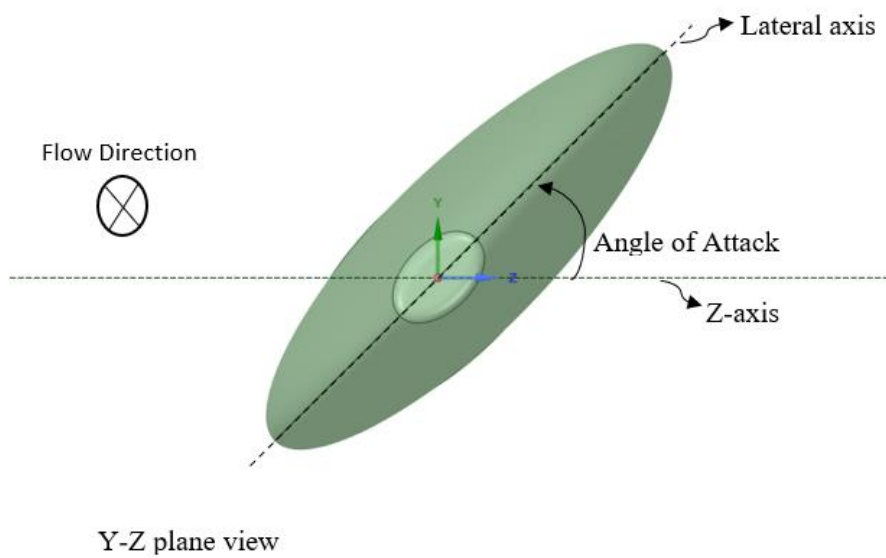


Figure 1.12 Angle of attack

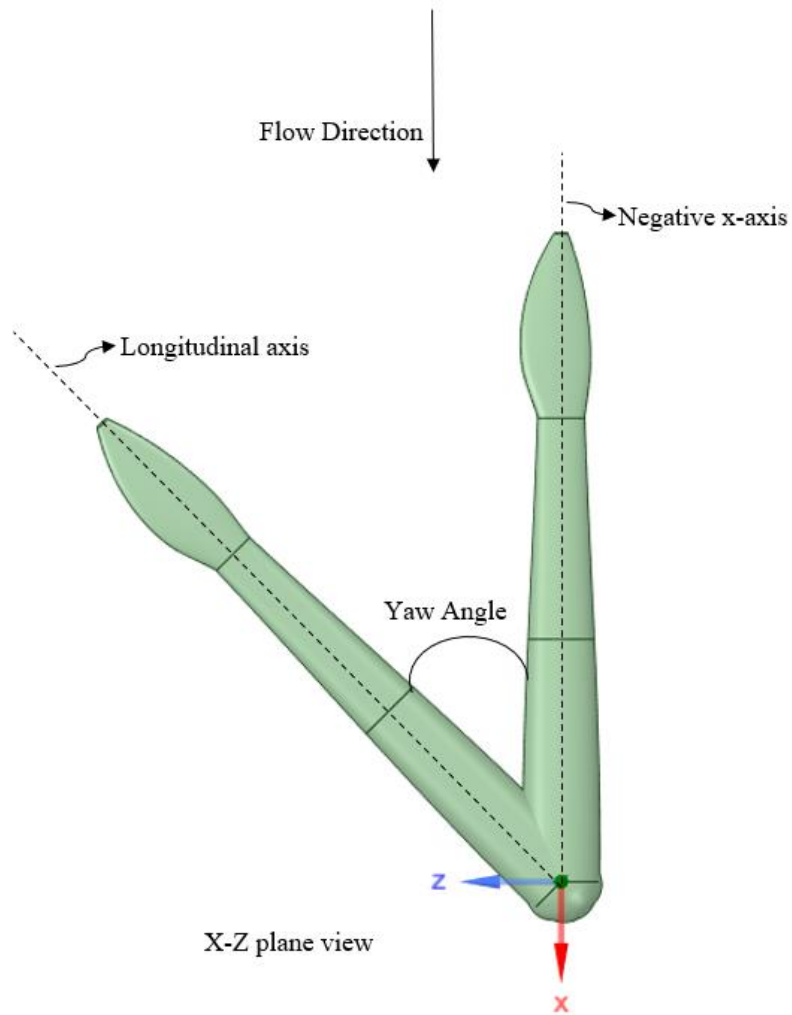


Figure 1.13 Yaw angle

For this study, only the change in the sweepback angle is considered. Values of angle of attack and yaw angles are selected as zero throughout this study.

1.3 Outline of the Thesis

This thesis consists of five chapters. Chapter 1 gives brief information on the physics of swimming and swimming styles. Then, it focuses on the front crawl swimming technique and its physics.

Chapter 2 presents the literature on experimental and CFD studies, unsteady flow analysis ,and turbulent flow selections on front crawl swimming.

The geometric details of the straight and angled arm models, numerical and visual details of the simulations of the mesh structure and the CFD model are provided in Chapter 3.

In Chapter 4, the results of the simulations of 12 swimming cases are given. First, propulsive force comparison of swimming cases is provided, then the pressure and velocity fields are examined for the straight and angled arms.

This thesis ends with major conclusions and future work ideas in Chapter 5.

CHAPTER 2

LITERATURE REVIEW

The goal of this thesis is finding the propulsive force generated by the arm and hand during front crawl swimming. This chapter looks at various literature on both computational and experimental studies of hand, forearm, and/or total arm in swimming, because it aims to understand how the two methodologies were utilized to investigate the subject. Looking at the relevant literature guided this study to determine the most fitting and feasible research approach. This chapter is divided into three sections: (1) CFD and Experimental, (2) Steady vs Unsteady, and (3) Turbulence Modeling. The first section explores CFD approaches and experimentation - the most commonly used methodologies of fluid dynamics in front crawl swimming. The second section looks into the time dependency of flow analysis of front crawl swimming. The last section investigates which turbulence model is the most suitable model for this study. These three parameters mentioned above are significant key factors for the flow analysis of front crawl swimming.

2.1 Computational and Experimental Studies

The first studies of swimming in the field of fluid dynamics started with the use of experimental techniques. Researchers have aimed to create an environment (involving mostly water and in some cases air) that is close to the real-life swimming environment in order to find the most accurate results of hydrodynamic forces acting on a swimmer's hand and/or arm. While some researchers conducted towing tank experiments [4]; [5]; [16], others did water channel experiments [2]; [3], in both cases, obtaining force measurements acting on a hand and/or arm model. In towing tank experiments, the model is pulled through the water at a certain speed while

water is stationary. On the other hand, in water channel experiments, the model is kept still while water is forced to flow around it.

In some experimental studies, an artificial hand and/or arm model is used to measure the forces acting on it in water. For instance, Berger et al [4] uses a combined hand and forearm model attached to a triangular towing carriage and dynamometer to examine the drag and lift forces acting at different angles. Their results show that drag force is maximum when the hand is almost perpendicular to the direction of motion and the lift force acts like a sinewave reaching maxima at different angles. For future work, this study points out the importance of finding the optimum hand orientation and movement so that the sum of drag and lift forces i.e. normal and tangential forces are maximum in the forward direction of swimming. Sanders' study [5] uses a hand model attached to a column apparatus, which focuses on the changes in drag and lift forces around a swimmer's hand by changing sweepback and angle of attack.

Sanders' findings reveal that when the sweepback angle is close to 90 degrees, the maximum force occurs, which is mostly generated from drag force. Furthermore, lift force contribution is significant when the sweepback angle reaches 45 degrees and angle of attack are close to 45 and 135 degrees. Their work finally suggests that further research should be conducted to check the importance of acceleration to create propulsive force and lift force to optimize swimming performance.

In another study, Sidelnik and Young [16] use a hand model attached to a carriage and column apparatus with a two-axis motor and load cell (Fig 2.1), which investigates how propulsive force can be affected by finger spreading. Their results show that 10° finger spreading creates more propulsive force than 0° finger spreading. More hand and stroke positions should be investigated to obtain more precise propulsive force values.

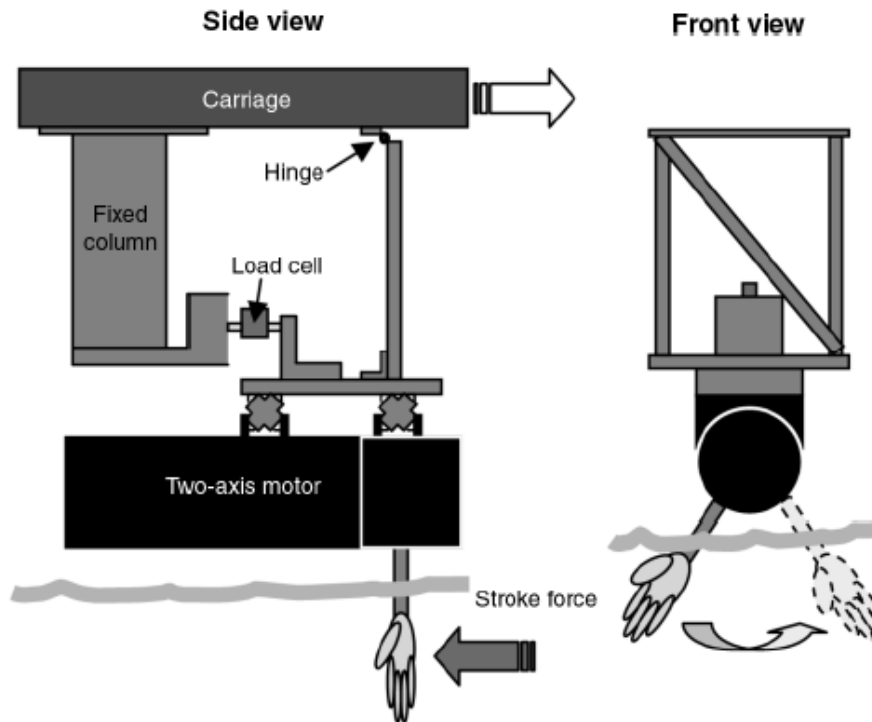


Figure 2.1 Test apparatus of Sidelnik and Young [16]

Rather than a simple hand model, Takagi et al. [17] uses a more sophisticated robotic hand and forearm device to better mimic swimming motion (Fig 2.2), which investigates 2D hydrodynamic forces acting on the hand and forearm. The experiment reveals that when the hand movement changes its direction, it results in a bound vortex circulation and during linear motion with the angle of attack, this also creates another circulation (Fig. 2.3). As a result of these two vortices, drag and lift forces occur, which contribute to the thrust force. The study further suggests that creating a 3D flow analysis is necessary to better understand hydrodynamic forces.

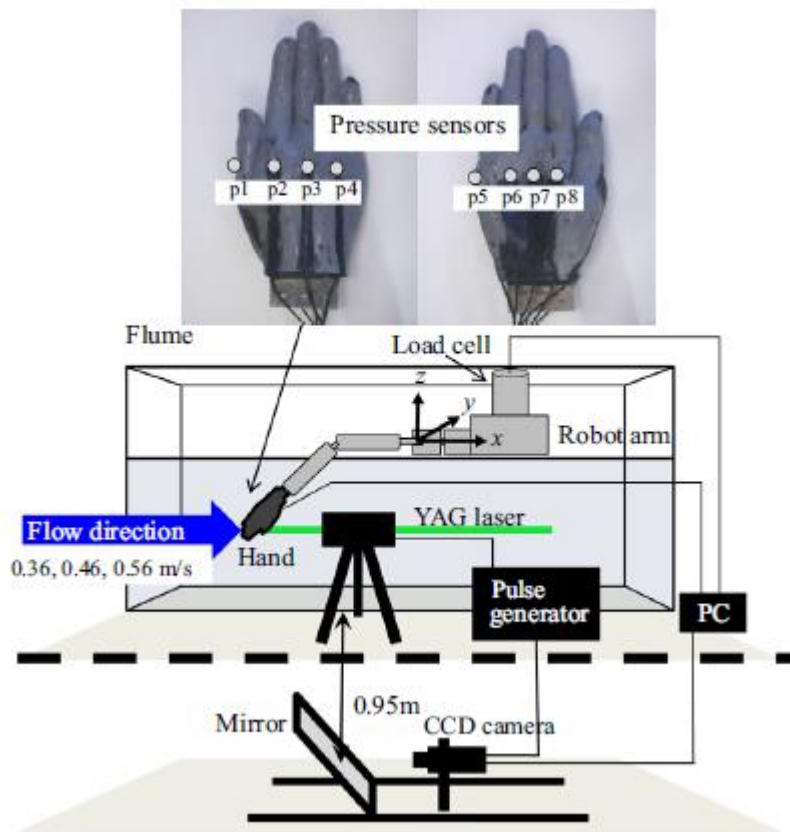


Figure 2.2 Test apparatus of Takagi et al. [17]

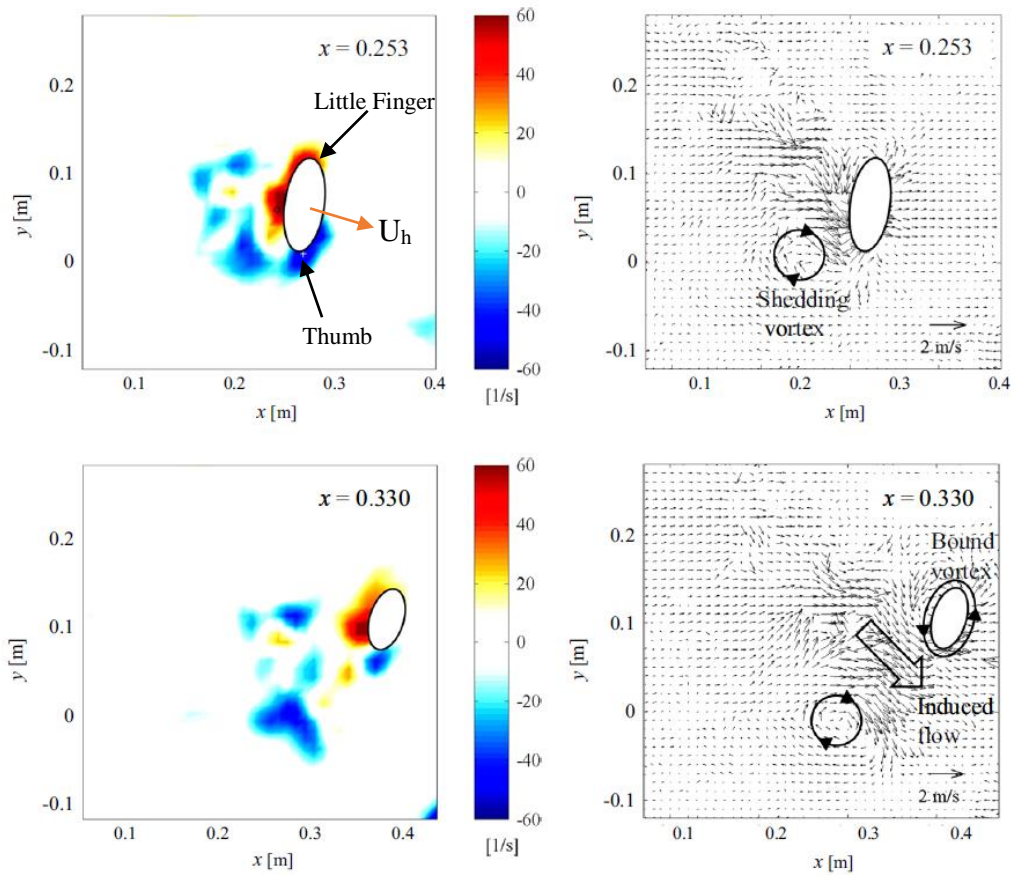


Figure 2.3 Vorticity distribution (left) and velocity distribution (right) of Takagi et al. [17]. There is a 67 ms time difference between the top and bottom instances. At the moment in the top figure, shedding vortex occurs due to the motion in the x -direction. At the moment in the bottom figure, in addition to the shedding vortex, a bound vortex occurs when a movement in z -direction occurs in addition to x -direction movement.

For some experimental research, real swimmers' hands and/or arms are preferred. For example, in Takagi and Sanders' [3] water channel experiment, real-life subjects are used by attaching micro pressure sensors to the right hands of three competitive swimmers and three novice swimmers. Their purpose is to understand propelling technique quantitatively by determining forces due to the pressure on the swimmers' hand. Their results reveal that not only the magnitude of the forces, but also direction of the forces is an important factor to take into account for swimming research. Other

than micro pressure sensors, an optoelectronic system is also used in experimental studies in swimming. For instance, Samson et al.'s study [18] tries to explain the relationship between kinematic hand parameters, which are angle of attack, sweepback angle, hand velocity, acceleration, and propulsive forces. They use 17 elite swimmers during three different distance swims: sprint, middle, and long distance. They mark seven locations on the hand to measure data by using an optoelectronic system. The authors find that the propulsive force reaches a maximum during push phase for sprint distance. Mean velocity values of the long distance, middle distance, sprint distance swims are 1.4, 1.5, and 1.6 m/s respectively.

In addition to micro pressure sensors and the optoelectronic system, video cameras are also used for experiments involving human subjects, such as, by Gourgulis et al. [19] (Fig 2.4). Their purpose was to find relative contribution of drag and lift forces and the effect of the hand's acceleration to the propulsive force. Their findings suggest that swimmers should accelerate their hands from the beginning of their backward motion, press the water with large sweepback angles during the middle part and sweep with small sweepback angles during the final part of their underwater arm stroke.

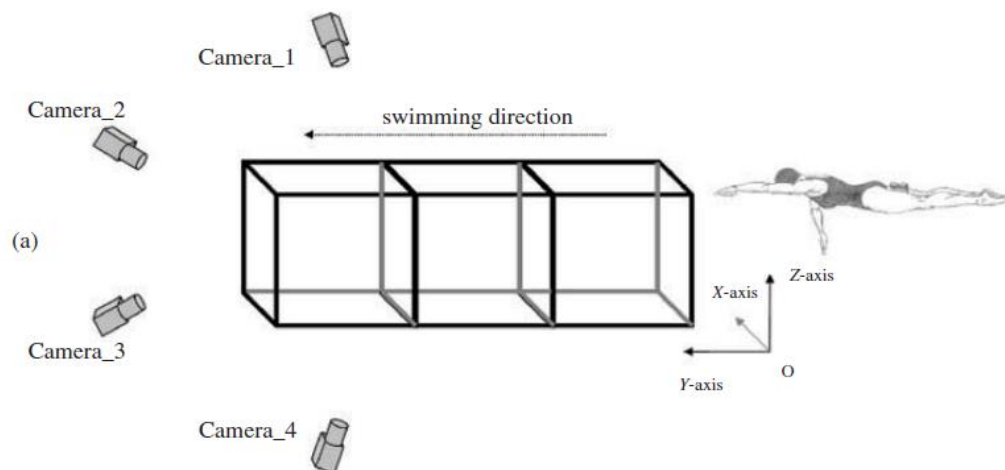


Figure 2.4 Video cameras and the human subject in Gourgulis et al. [19]

Unlike experiments, CFD creates a mathematical model and uses numerical techniques to perform flow analysis. First CFD analyses on swimming tried to compare their results with experimental studies so as to prove that CFD can also find accurate results and become a useful tool for swimming research. Following this purpose, Bixler and Riewald [12] conducted a CFD analysis and compared their findings with Berger et al.'s [4] towing tank experiment, in which the peak lift force due to the changing angle of attack was observed at approximately the same angle in both studies. Also, both the CFD and experimental research reached the same outcome: the hand segment is the main contributor to the lift force. Roubua et al. used 2D [13] and 3D [14] hand/arm models in their CFD research and compared their results with Berger et al.'s [4] and Sanders' [5] towing tank experiments to see a similar trend: Drag coefficient is maximum when the angle of attack is 90 degrees, which means that CFD can give similar results with experimental research for accelerated flow conditions which means the flow velocity increases with time.

There are also CFD studies that are compared with water channel experiments. For instance, Bilinauskaite et al. [20] compared their findings with Schleihauf's water channel experiment [2], and showed that for both studies drag coefficients have the same increase-decrease trend (Figure 2.5). For example, when Scheleihauf's study [2] reaches maximum drag coefficient at 2 m/s with 0° sweepback angle and 55.5° angle of attack, Bilinauskaite et al.'s study [20] has a close coefficient value at the same velocity and angle of attack values. On the other hand, Bilinauskaite et al. [20] reaches the maximum drag coefficient when the velocity is 1.82 m/s, at 140.8° sweepback angle, and at 50.3° angle of attack. From the last two data points in Fig 2.4, although angle of attack changes from 25.1° to 20.7°, drag coefficients does not have a significant change for both studies. This may be due to the sweepback angles remaining the same for both studies. Thus, it may be deduced that the sweepback angle has more impact than the angle of attack on drag coefficient.

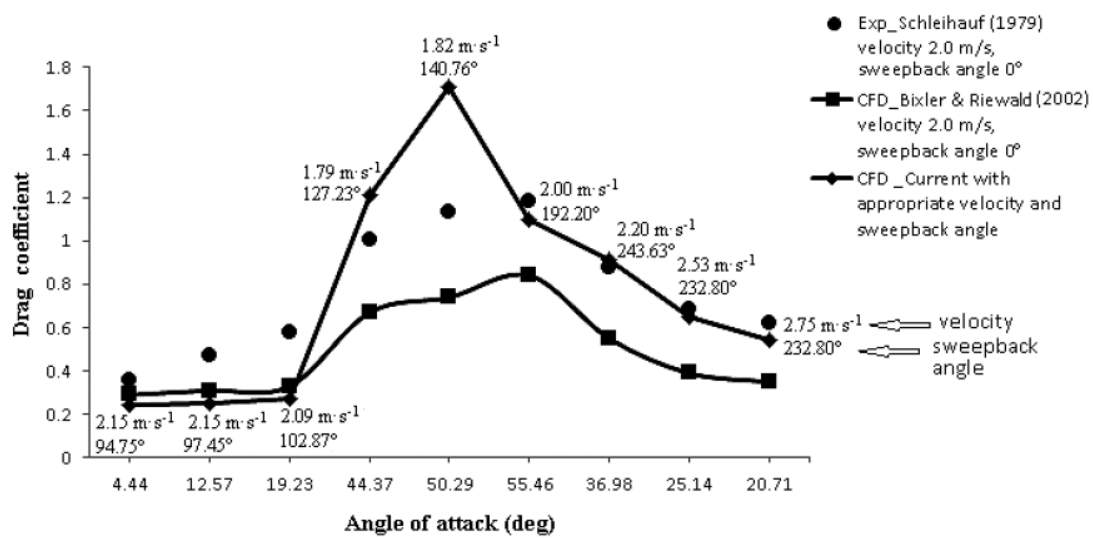


Figure 2.5 Variation of drag coefficients with angle of attack in Schleihau [2] and Bilinauskaite et al. [20]. Bilinauskaite et al. [23] uses appropriate velocity and sweepback angle values in order to compare their study with Bixler and Riewald [12] and Schleihau [2]

Another example is the comparison of Samson et al.'s CFD analysis [21] with Takagi et al.'s experimental study [17], where similar results can be observed despite implementing different methods for obtaining data. Both studies show that vortex shedding was responsible for the increase of propulsive force at same instantaneous time (Samson et al., [21], p. 792). The shed vortices, one clockwise and one counterclockwise, result in a pressure difference between the dorsal and palm side

of the hand. Then, the pressure difference leads to the drag force, which contributes to the propulsive force (Fig. 2.6).

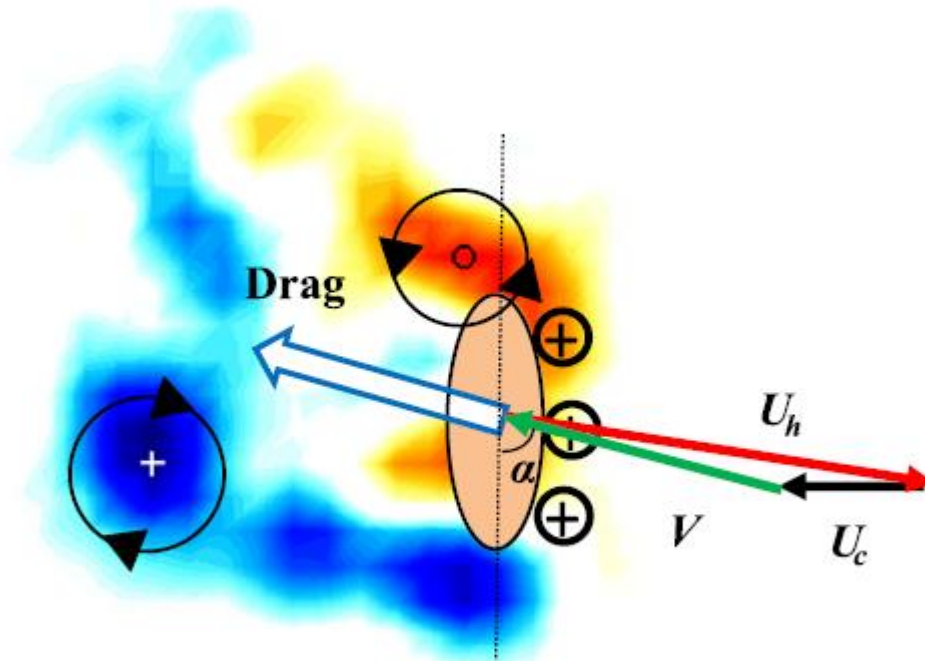


Figure 2.6 Two vortices lead to the drag force for Takagi et al. [17] and Samson et al. [21]. Red color indicates counter-clockwise vortices and blue is for clockwise [17].

Lecrivain et al.'s study [22] focuses on the hydrodynamic forces acting on the total body and upper arm of a swimmer, who has an arm amputation at the level of the elbow. They scan the geometric data of a female swimmer's body in order to create a solid surface of it using reverse engineering. In their simulation, they change body rotation and arm rotation in order to mimic swimming motion using dynamic mesh approach in Fluent 6.3. They cannot compare the results with literature due to not having any literature that focuses on the forces acting on only upper arm. First, they make a steady flow analysis to create drag force and then they use the outputs of this simulation in unsteady flow. The authors emphasize that CFD simulations can lead to flow visualization anywhere in the solution domain and any time during unsteady

analysis, which is an advantage of CFD over experimental studies. Inlet velocity is selected as 1 m/s by referencing an article that mentions this as a common swimmer's speed. This article illustrates that upper arm also has a contribution to the propulsive force during front crawl swimming.

By looking at the current literature mentioned above, it can be seen that despite not having an experimental setup and even a real human subject, CFD can produce similar results solely through numerical simulation. Thus, it can be deduced that CFD can be a useful tool in terms of getting results of a flow in different locations and time inside solution domain and ease of calculation of hydrodynamic forces and coefficients for swimming research.

2.2 Steady vs Unsteady Simulations

Time dependency of a flow is another significant concept to take into consideration in order to model front crawl swimming. In steady flow, flow properties such as velocity and pressure may change from one spatial point to another, but they do not change with time. On the other hand, in unsteady flow, fluid flow properties are affected by the time change. This section will examine the literature on the steady and unsteady flow in front crawl swimming and attempt to understand the outcomes of applying two different flow conditions to the front crawl swimming research.

Comparing steady and unsteady conditions in swimming research shows that implementing unsteady conditions is a more suitable approach because real-life swimming involves unsteady effects, such as acceleration, hand-arm movements, and vortices. For instance, Rouboa et al.'s CFD study [13] first made a steady flow analysis in order to compare their results of drag and lift coefficients with experimental studies; however, the analysis lacked the effects of flow acceleration to drag and lift coefficients, which eventually led them to conduct an unsteady flow analysis. The comparison of both analyses shows that more propulsive force (approximately 22.5%) could be produced under the accelerated flow condition,

which can be better predicted in unsteady flow analysis than in steady flow analysis. Rouboa et al. [13] emphasize that in addition to flow acceleration, including multi axis rotations to the hand and/or arm movements is also necessary in order to better model swimming, which can be done in unsteady simulations. Another CFD study by Sato and Hino [23] utilizes the unsteady flow condition to compare the differences in stroke types of two different top swimmers during front crawl swimming, because unsteady flow condition is able to check small differences of their stroke types within small time differences. Thus, unsteady flow analysis enables the researchers to better predict velocity and pressure differences on these two swimmers' hands.

Experimental and CFD studies mostly prefer unsteady flow analysis because it creates more realistic swimming conditions. For instance, Gourgulis et al.'s experimental study [19] investigates accelerations of ten female swimmers' hands via four video cameras and mentions that it is experimentally difficult to analyze unsteady underwater movements in a swimming pool to understand vortex shedding effects on propulsive force. From these results, unsteady effects such as vortex shedding also have impact on propulsive forces and need to be examined in a computational environment such as CFD. Kudo et al.'s experimental study [24] uses human hand as model in a small-scale water channel. Hydrodynamic forces are examined for angular motion first without an inlet velocity and then with 1 m/s and 1.5 m/s inlet velocity. The researchers mention that continually changing the orientation of the hand may affect additional vortex formation. They say that impulsive start of the hand model may accelerate the fluid around it, creating added mass effect. Another interesting finding of this research is that even during deceleration, drag force in accelerated flow is bigger than non-accelerated flow. This result is attributed to the great vortex generation during that acceleration and deceleration. Thus, one needs to look at added mass effect and vortices both in order to understand the reason for existence of drag force which also means propulsive force.

Cohen et al.'s CFD analysis [25] of full-body movement in front crawl swimming also uses unsteady flow analysis because unlike steady analysis it can show the thrust force in the effect of time differences. Gardano and Dabnichki [7] performed an experimental and CFD study using a quasi-steady approach to find drag and lift forces. First, they use a male swimmer's full arm model in a low-speed wind tunnel with 135°, 160° and 180° degrees for elbow angles. For each elbow angle, angle of attack varies between 0 and 140° with an increment of 10°. The results show that maximum drag force is achieved when the elbow angle is 160°. They suggest that unsteady flow characteristics are important to accurately find drag and lift forces for different elbow angles. Furthermore, Dabnichki's CFD study [26] focuses on how added mass concept can affect the torque on the shoulder joint. However, this research did not consider vorticity effects during swimming. Even some steady flow analyses indicate that body movements, mostly hand and/or arm movements, should be realistically investigated by using unsteady flow conditions. For example, as mentioned in Section 2.1, Berger et al.'s steady state experimental analysis [4] comments that it is important to understand the effect of drag and lift coefficients during real-time swimming. Modelling real-time swimming requires considering unsteady effects such as real-time movements, accelerations, decelerations, and orientations. Bazuin's [27] steady state experimental study also shows that steady state flow condition is not adequate to show instantaneous flow change around swimmers' hands. Even though steady flow conditions can provide comparable data with experimental studies, unsteady flow analysis is a more useful tool to calculate the accelerations, hydrodynamic forces, and coefficients during body movements for swimming research.

Van Houwelingen et al.'s quasi-steady CFD study [28] looks at four different finger spreading angles to check how much drag force is created during front crawl swimming. For this purpose, they use a hand and forearm model in numerical simulation and in a wind tunnel. The results show that for each finger spreading angle case, drag coefficient is greater than the closed finger model (0-degree finger spreading). Furthermore, they mention that using the optimal finger spreading angle

during front crawl swimming can lead to 5 % advancement in propulsion. When they calculate the power that swimmers need to overcome the drag and create propulsion by the hand/arm segment, they find that 430 W is needed. This 5 N advancement in propulsion can lead to increasing the swimmer's speed from 2 m/s to 2.2 m/s. This velocity increase and power expenditure enables the swimmer to improve his/her best personal time 0.6 s for 50 m front crawl swimming. This time improvement may help a swimmer to get a higher position in a swimming competition. This paper also suggests an unsteady flow analysis to better understand flow characteristics rather than looking at the snapshot of a stroke.

Gomes and Loss' study [29] is a review on swimming propulsion research in literature. Their main purpose is to show the unsteady effects of swimming propulsion by looking at the studies that show steady and unsteady analysis comparison. They select six works that use at least one unsteady effect on swimming propulsion such as accelerated flow and hand orientation in experimental or computational study. Gomes and Loss [29] point out that although the results show that unsteady flow conditions can create more propulsion than the steady flow conditions, the reason is still not completely explained. They emphasize that literature has little knowledge on the mechanisms of increased propulsion and the most effective swimming technique. Therefore, Gomes and Loss [29] suggest more studies on unsteady flow conditions to better understand swimming propulsion.

2.3 Turbulence Modelling

The flow regime which includes characteristics such as mixing, swirling and rapid variation in flow velocity and pressure is called turbulent flow. On the other hand, if the flow regime has regular characteristics and less fluctuation, then it is called laminar flow. The arm movements during front crawl swimming bring about chaotic changes in flow variables, which as a reaction, affect the swimmer's speed and propulsive force. Thus, front crawl swimming by its nature has these chaotic flow characteristics (Fig. 2.7), which is why implementing a turbulence model to the flow

simulation of front crawl swimming instead of a laminar model would show more accurate results.



Figure 2.7 Arm strokes can create flow mixing and swirling during front crawl swimming

There are two common turbulence models used in swimming research: k-epsilon (ϵ) and k-omega (ω) SST. The k- ϵ turbulence model is generally preferred for external flow around complex geometries because of its good convergence behavior and low memory requirements [30], thus, some of the studies prefer this turbulence model ([12], [13], [20]). On the other hand, the k- ω SST model provides a better prediction of flow separation than k- ϵ model and also accounts for its good behavior in adverse pressure gradients [8], thus, some research prefers this turbulence model ([21], [27]). As it will be observed in the presented research below, the k- ω SST turbulence model is more suited for simulating front crawl swimming.

Even the results of some studies using laminar models show that using an accurate turbulence model is necessary. For example, Sato and Hino (2013), who use a laminar model, state that flow separations occur at the edge of hands independent of Reynolds number (p. 681); however, there are flow mixing vortices in their results and flow separation delays might have occurred due to the turbulent flow regime. Therefore, choosing a turbulence model, which yields more accurate results close to the hands is necessary for front crawl swimming. We can also understand if the selected turbulence model is accurate enough by comparing turbulence model simulations with sound experimental studies. For instance, Bazuin (2018) compared $k-\epsilon$ realizable, $k-\epsilon$ and $k-\omega$ SST models with their experimental data in terms of finger spacing and drag coefficient relationship. Their results for $k-\omega$ SST show that drag coefficient decreases when spacing increases, which is in a similar trend with the experimental study. Therefore, $k-\omega$ SST could be the most suitable model to understand finger spacing for simulating front crawl swimming. In conclusion, the research presented above shows that even though the $k-\epsilon$ model is more convenient due to its good convergence and low memory requirement, $k-\omega$ SST is the most ideal model because it creates a more accurate simulation of flow regime of front crawl swimming.

2.4 Summary of the Literature

Table 2.1 summarizes literature on some CFD studies on human swimming. Most of the research use ANSYS Fluent as CFD code. Some of the research prefer in-house codes or other software packages such as STAR-CCM+. Hand is the most preferred model object in swimming research due to having more examining parameters such as finger spread and thumb abduction/adduction. Forearm and full arm are also selected by some studies in order to have more realistic approach. Circular disk is another object considered in the swimming research in order to have a simple model that imitates human hand. All of steady, quasi-steady and unsteady flow analyses are preferred in order to have simple or more realistic approach. 3D models are created

more than 2D ones because it is hard to simplify human limbs as 2D. Although the studies use different characteristic lengths, such as length of the hand and length of the full arm, 10^6 and 10^7 are the most observed Reynolds Number for the studies. $k-\epsilon$ turbulence model is the most common turbulence modeling option. However, recent studies prefer $k-\omega$ SST turbulence model. Most of the studies emphasize looking into unsteady effects during swimming as a future work.

Table 2.1 CFD research related to front crawl swimming

Article	Software	Objects	Steady/Unsteady	2D/3D	Reynolds Number	Turbulence Model	Results/Conclusions
Bixler and Schloder (1996)	Fluent	Disk	Steady	2D	N/A	k-ε, RNG and RSM	Propulsive drag increases under accelerated conditions
Bixler and Riewald (2002)	Fluent	Hand, Forearm	Steady	3D	10^7 to 10^8	k-ε	Drag is bigger than lift and maximum at 90° angle of attack and lift is maximum at 55° and 140°
Sato and Hino (2003)	SURF (in-house solver)	Hand	Unsteady	3D	$\sim 2 \times 10^5$	No Turbulence Model	Unsteady CFD simulation is required instead of a quasi-steady method for the analysis of practical swimmer's strokes.
Rouboa et al. (2006)	Fluent	Hand, forearm	Both	2D	10^7 to 10^8	k-ε	Unsteady conditions have more propulsive force than the steady conditions
Gardano & Dabnichki (2006)	Fluent	Full arm	Quasi-steady	3D	1.5×10^7 to 2×10^7	N/A	Unsteady flow characteristics are important to investigate to accurately find drag and lift forces for different elbow angles
Lecrivain et al. (2008)	Fluent	Full body, upper arm	Unsteady	3D	N/A ($V = 1m/s$)	N/A	Upper arm has also a contribution to the propulsive force.
Marinho et al. (2009)	Fluent	Hand	Steady	3D	10^5 to 10^6	k-ε	Drag coefficient is higher when thumb is adducted. Lift coefficient is increases during fully abducted at angle of attacks 0° and 45°
Marinho et al. (2010)	Fluent	Hand	Steady	3D	$\sim 4 \times 10^5$	k-ε	Fingers slightly spread creates more resultant force. Future work is needed for unsteady effects such as accelerations, decelerations, and rotations
Loebbecke and Mittal (2012)	In-house solver	Full arm	Unsteady	3D	10^4	N/A	Their "lift" definition is a major contributor to thrust, also in a "drag-based" technique.
Bilinauskaite et al. (2013)	Fluent	Hand	Quasi-steady	3D	$\sim 10^6$	k-ε	Hand shape, velocity, orientation affect drag force
Sato and Hino (2013)	In-house (SURF)	Hand	Both	3D	10^5 to 5×10^8	N/A (Laminar)	Average propulsive force is 63.9_N for a swimmer at 1.84 m/s.
Samson et al. (2017)	STAR-CCM+	Hand, forearm	Unsteady	3D	$\sim 10^6$	k-ω SST	Two peak forces during the IN and UP phases. Hand contributes to propulsion more than forearm.
Beaumont et al. (2017)	Fluent	Full Body	Steady	3D	$\sim 10^7$	k-ω	For all cases, lower pressure area occurs behind of the swimmer. Also, side parts of the swimmer have lower pressure area relatively smaller region than the behind part of the swimmer.
Bazuin (2018)	Fluent	Disk	Steady	3D	10^4 to 10^6	k-ε, Realizable k-ε, k-ω SST	Simple simulations on slotted disks are not a viable option to represent hands with finger spreading.

Table 2.2 summarizes experimental studies on human swimming. Water channel, towing tank, wind tunnel, PIV and optoelectronic method are used as experiment methods. The research generally focuses on the relationship among kinematic parameters, model shape and hydrodynamic forces. It is observed and even some of the research suggest that more parameters and data are needed to understand how hydrodynamic forces can be affected by changing kinematic parameters.

Table 2.2 Experimental studies on human swimming

Article	Method	Research Focus	Results/Conclusions
Schleihauf (1979)	Force measurement on hand model in water channel	Steady state hand orientation and finger spread analysis	Hand shape affects drag and lift coefficients
Berger et al. (1995)	Force measurement on hand model in towing tank	Finding drag and lift forces by changing angle of attack and sweepback angles	Drag is maximum when the velocity vector is almost perpendicular to the model. On the other hand, lift has two maxima at 55 and 155 degrees angle of attack.
Sanders (1999)	Force measurement on hand model in towing tank	Hand orientation and acceleration effect on drag and lift forces	Drag contribution is significant. Maximum force close to sweepback angle 90. Lift force contribution is important at sweepback angle 45 and angle of attack 45 and 135 degrees
Takagi and Sanders (2002)	Swimmer in water channel pressure measurement	Stroke and force analysis of four different level of swimmers	Pressure transducer method and qualitative video analysis are useful tools. Not only the magnitude of the forces, but also the direction of the forces is an important factor to take into account for swimming research.
Sidelnik and Young (2006)	Force measurement of hand model in towing tank	Finger spread effect on propulsive force	More hand and stroke positions should be investigated to obtain more precise propulsive force values
Gardano and Dabnichki (2006)	Force measurement of full arm model in wind tunnel	Flow analysis of different elbow angles	160° elbow angle creates more drag force than the other elbow angles
Kudo et al. (2013)	Force measurement of hand model in a swimming flume	Flow analysis of angular motion of hand with and without inlet velocity values	Impulsive start of the hand model may accelerate the fluid around it thus this creates adding mass effect. Even during deceleration drag force in accelerated flow is bigger than non-accelerated flow
Gourgoulis et al. (2014)	Kinematic data obtaining from video cameras	Hand's acceleration effect on propulsive forces in different swimming phases	Swimmers should accelerate their hands from the beginning of their backward motion, press the water with large sweepback angles during the middle part and sweep with small sweepback angles during the final part of their underwater arm stroke.
Takagi et al. (2014)	Water channel+robotic arm using PIV	Investigating hydrodynamic forces acting on hand	When the hand movement changes its direction, it results in a bound vortex circulation and during linear motion with the angle of attack, this also creates another circulation
Samson et al. (2015)	Optoelectronic system on 7 marked locations on hand	Explain the relationship between kinematic hand parameters and propulsive force	Propulsive force reaches maximum during upsweep phase for sprint pace
Bazuin (2018)	Hand/forearm model in wind tunnel	Finding drag and lift coefficients using different finger spreading	It is advised to make a swimmer's hand as flat as possible, while simultaneously maintaining a 5° finger spreading, as this maximizes drag forces according to all different analysis on force coefficients

CHAPTER 3

CFD MODEL

This research involves CFD analyses in order to investigate propulsive force during front crawl swimming. For this purpose, two common arm positions in this swimming technique are investigated by changing the elbow angle. While doing this, three different swimming velocities and three different rotational arm velocities are examined for the two elbow angles. The chapter is divided into four sections: (1) Geometry Creation, (2) Solution Domain and Boundary Conditions, (3) Mesh Independence Study, (4) CFD Setup, and both elbow angles are investigated within these sections.

3.1 Geometry Creation

For CFD simulations, creating the corresponding geometry is an important concept. Geometry defeaturing can enable one to easily create high quality meshes around geometries. However, geometry defeaturing process must not interfere with the reality of the geometry. Based on these, CFD models of human right arms with 0° and 55° elbow angles are created.

Arm measurements are taken from different references. For total arm length, Singha et al. [31] is considered, who measured total arm length as 78.2 cm. Hand thickness, elbow and upper arm width is selected as 2.9 cm, 8.4 cm and 9.0 cm, respectively [32].

Geometry creation of the straight arm is done by the help of ANSYS SpaceClaim Computer Aided Drawing (CAD) Software. Length of the hand segment is 21.6 cm, arm segment, including shoulder head, is 59 cm, thus; total model length is 80.6 cm

which is a close value to total arm length of Singha et al. [31]. Different views of the straight arm model can be seen in Fig. 3.1.

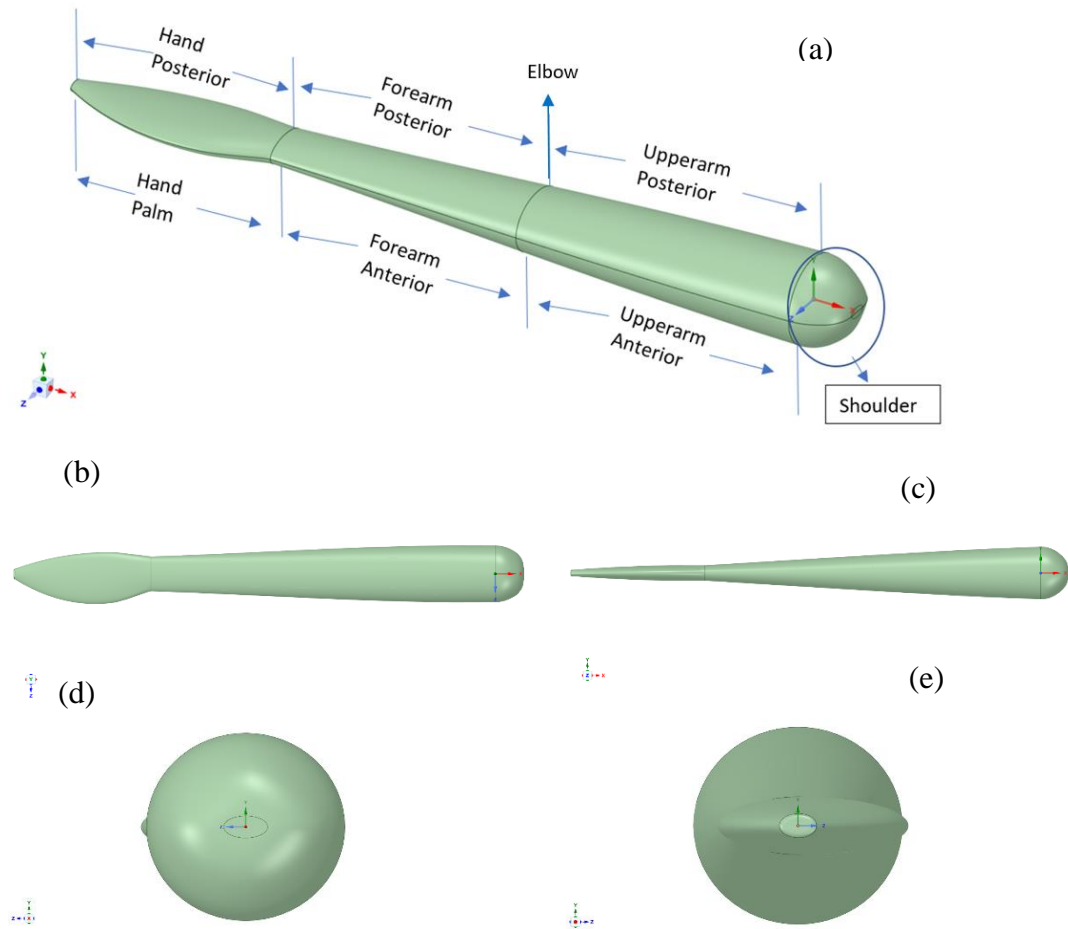


Figure 3.1 Different views of the straight arm model. (a) Parts of the straight arm model (b) Top view of the straight arm model. (x-z plane) (c) Front view of the model. (x-y plane) (d) Close view to the shoulder of the straight arm model (z-y plane) (e) Close view to the tip of the hand of the straight arm model

The straight arm model consists of anterior and posterior parts of the hand, forearm, upper arm, including the elbow between the forearm and the upper arm, and the shoulder (Fig 3.1(a)). Since the model is drawn by taking the human right arm as an example, the width of the hand in the +z direction is drawn longer than the width in the -z direction in order to show the effect of the adducted thumb on the model (Fig

3.1(b)). The thickness of the hand is drawn (Fig 3.1(c)) by considering [32]. Tip of the shoulder consist of a relatively small elliptic surface area to better imitate the human shoulder (Fig 3.1(d)). In addition to the tip of the shoulder, tip of the hand also consists of an elliptic area, but rounded corners are made for this elliptic area in order to have smooth fingertips (Fig 3.1.(e)).

By bending the elbow of the straight arm model, elbow angled arm is created. To decide on the value of this elbow angle, Olympic swimmer Michael Phelps' front crawl swimming technique is examined and it is observed that 145° occurs between the forearm and upperarm (Fig 3.2), thus 145° elbow angle is chosen (Fig 3.3 and Fig 3.4).



Figure 3.2 145° elbow angle is observed in Michael Phelps' front crawl swimming technique

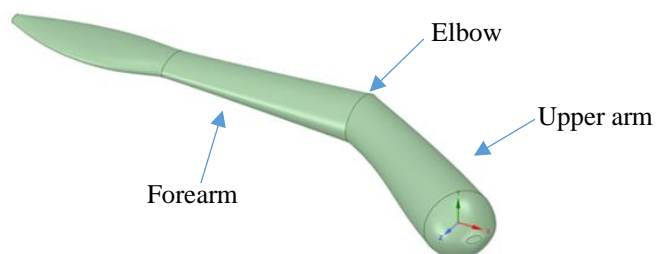


Figure 3.3 Elbow angle is created between the forearm and the upper arm

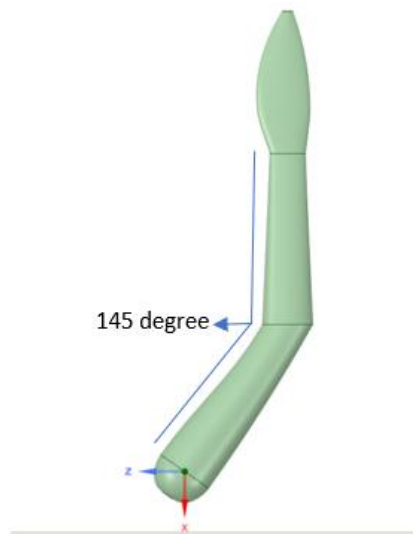


Figure 3.4 Elbow angle is 145°

3.2 Solution Domain and Boundary Conditions

For both straight angled arm models, the solution domain consists of two regions in order to use the sliding mesh technique: cylinder region and box region. Cylinder region, which is located inside the box region (Fig. 3.5) includes the hand/arm model in itself (Fig 3.6) and its center is located at the origin, which is also the center of the circular surface boundary between the shoulder head and the arm. In addition, the arm rotation center is chosen as this center and the hand/arm model rotates around the z-axis from this center. Figure 3.7 demonstrates how the size of the box region is selected according to the length of the hand/arm model. It is aimed that the boundary conditions be far enough from the hand/arm model so that the boundary conditions do not affect the flow. While doing this, the dimensions of the box region and the cylindrical region are determined after a series of preliminary studies, avoiding the possibility that the solution domain will be too large and thus, the calculation time would be prolonged. As a result, dimensions of the box region are $10L$ in length, $4L$ in height $4L$ in width, and the diameter and the width of the

cylinder region are $3L$ and 94 cm, respectively, where L is the length of the hand/arm model (Fig. 3.7).

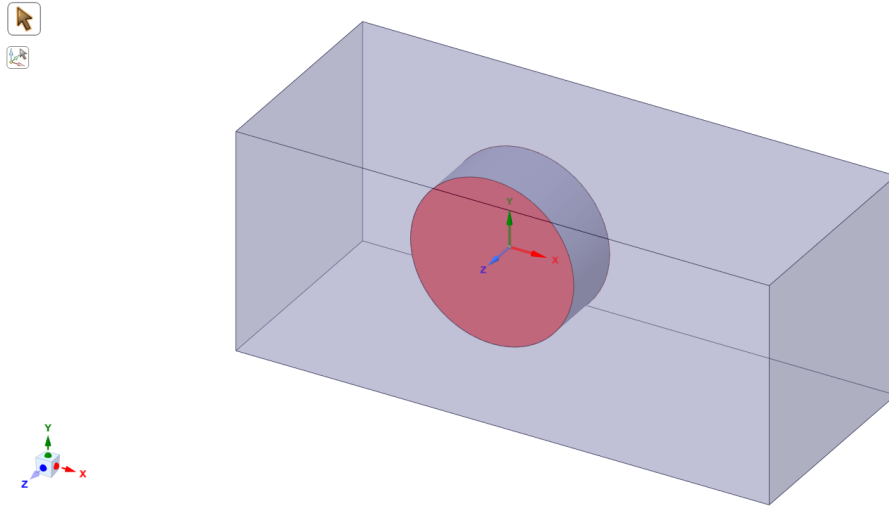


Figure 3.5 Cylinder region which has the hand/arm model in itself, is located inside the box region

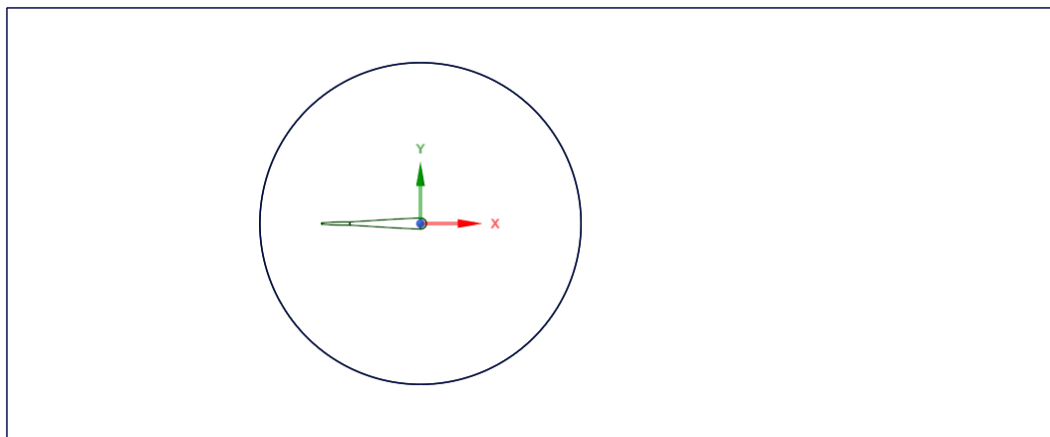


Figure 3.6 Hand/arm model location inside the solution domain

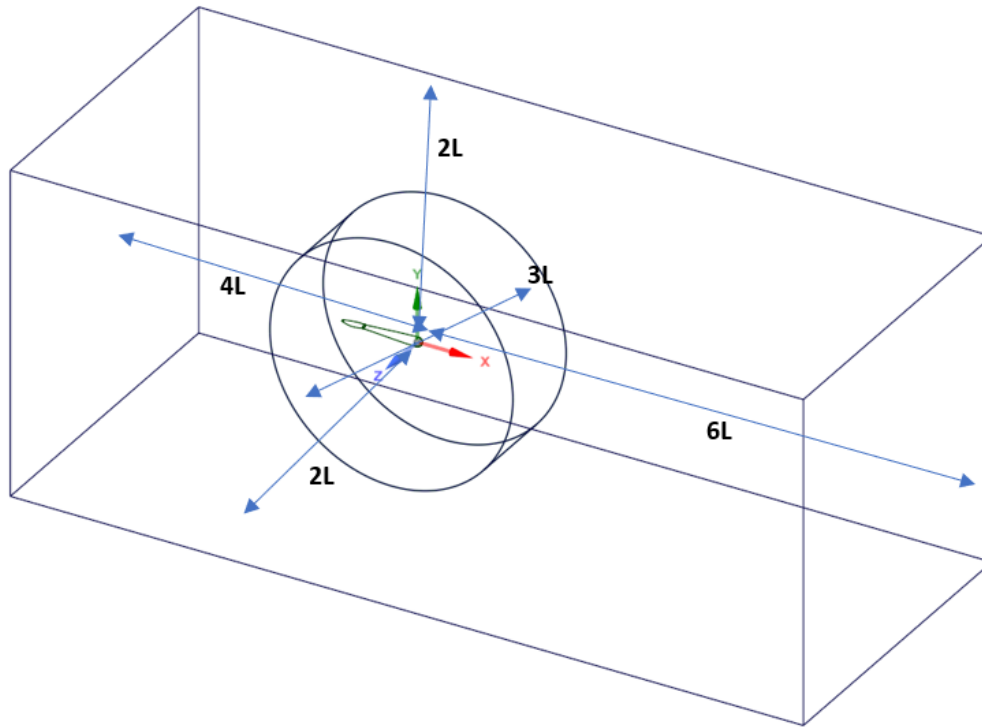


Figure 3.7 Solution domain measurements. L is the total arm length which is nearly 80 cm.

3.2.1 Investigated Cases and Boundary Conditions

Different swimming velocity (velocity in the forward direction) and rotational arm velocity cases are investigated in order to better simulate real swimming behavior during front crawl swimming. For swimming velocities, 1, 1.5, and 2 m/s are selected, because these values can be roughly categorized as slow pace (1 m/s), normal pace (1.5 m/s) and sprint pace (2 m/s) in front crawl swimming. Other than swimming velocities, rotational arm velocities can change during front crawl swimming and need to be examined. For this purpose, two stroke paces are investigated in this study: One full stroke phase in one second (3.14 rad/s), which mostly refers to normal pace of front crawl swimming and two stroke phases in one

second (6.28 rad/s), which can be seen in sprint races. Thus, every swimming velocity and rotational arm velocity cases are combined for each hand/arm model which are straight arm and elbow angled arm models. There are 12 investigated cases: 6 for the straight arm and 6 for the angled arm model. Table 3.1 presents the investigated swimming cases in this study. Swimming cases of the straight arm are denoted with 1, and the angled arm with 2. Then, for different cases of velocities, cases are coded with letters; A, B, C, D, E, F.

Table 3.1 Investigated swimming cases in this study

Case Code	Straight Arm (1)		Case Code	Angled Arm (2)	
	Swimming Velocity (m/s)	Rotational Arm Velocity (rad/s)		Swimming Velocity (m/s)	Rotational Arm Velocity (rad/s)
1A	1	3.14	2A	1	3.14
1B	1	6.28	2B	1	6.28
1C	1.5	3.14	2C	1.5	3.14
1D	1.5	6.28	2D	1.5	6.28
1E	2	3.14	2E	2	3.14
1F	2	6.28	2F	2	6.28

Figure 3.8 and Table 3.2 present the details of the boundary conditions. Velocity inlet is 4L away from origin on the left side of the box region, where the speed is specified as 1, 1.5 or 2 m/s depending on the simulated case. Turbulence intensity is selected as 5 % and turbulence viscosity ratio³ is 10, which are the default values in ANSYS Fluent. Gravity is neglected for this study. Pressure outlet is determined as

³ Turbulence intensities of 1 % or less than 1 % are considered as low, more than 10 % are considered as high. Therefore, for this study, at the beginning, a mean value of 5 % turbulence intensity is selected. Turbulent viscosity ratio of 10 is typically selected for external flows [31].

zero gage pressure on the right side of the box body. Top of the box is chosen to be zero shear wall (free surface) boundary by thinking it as a swimming pool surface. Bottom of the box has slip wall boundary condition to consider that the swimmer is moving forward relative to the bottom boundary. Thus, the bottom wall has the same value and direction with the velocity inlet. Front and back of the box region are considered as symmetry boundary condition. Hand/arm is selected as no slip rotational moving wall with 0 rad/s relative velocity to adjacent cells. Finally, interface condition is assigned to the interface between the cylindrical and box regions in order to simulate the sliding mesh approach.

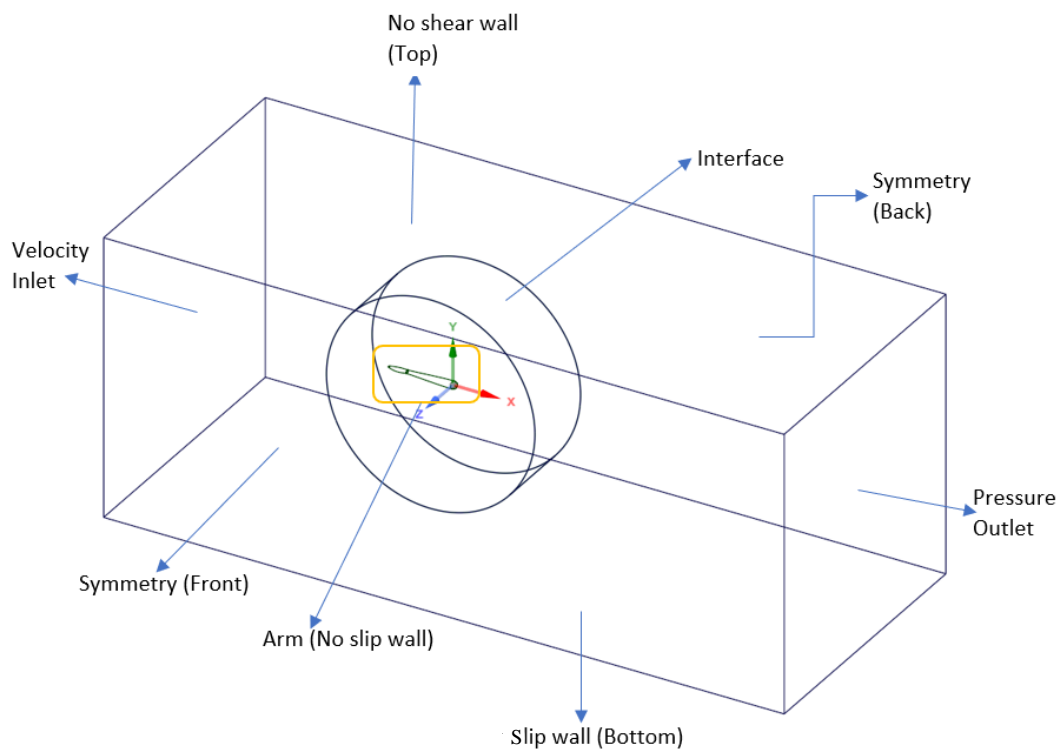


Figure 3.8 Boundary conditions

Table 3.2 Boundary conditions' details

Location	Boundary Condition Type	Parameter	Value
Inlet	Velocity Inlet	Velocity Magnitude (m/s)	1, 1.5 or 2
		Turbulence Intensity (%)	5
		Turbulence Viscosity Ratio	10
Outlet	Pressure Outlet	Gage Pressure (Pa)	0
Top	Zero Shear Wall (Free Surface)	-	-
Bottom	Slip Wall	Moving Wall Velocity (m/s)	1, 1.5 or 2
Front	Symmetry	-	-
Back	Symmetry	-	-
Arm	No Slip Rotational Moving Wall	Relative velocity to adjacent cells (rad/s)	0

3.3 Mesh Generation and Mesh Independence Study

Mesh generation is important for a CFD study in terms of accuracy, preparation and solution time. Creating a relatively coarse mesh near the boundary of interest may result in inaccurate results, however; redundantly fine mesh may cause too much computational time and memory allocation. For this study, it is important to create a fine mesh close to the hand/arm model to better simulate the flow around it. Figure 3.9 shows mesh structure of the solution domain selected after the mesh independence study (See 3.3.1 Mesh Independence Study). The mesh inside the box region gets denser close to the cylindrical region by assigning proper sizing to the interface between two regions. Figure 3.10 shows a close-up view of the mesh inside the cylindrical region. Shared topology is not selected for the interface between the cylindrical and box regions, because sliding mesh technique is used, and the cylindrical region rotates around the z-axis, whereas the box region is fixed.

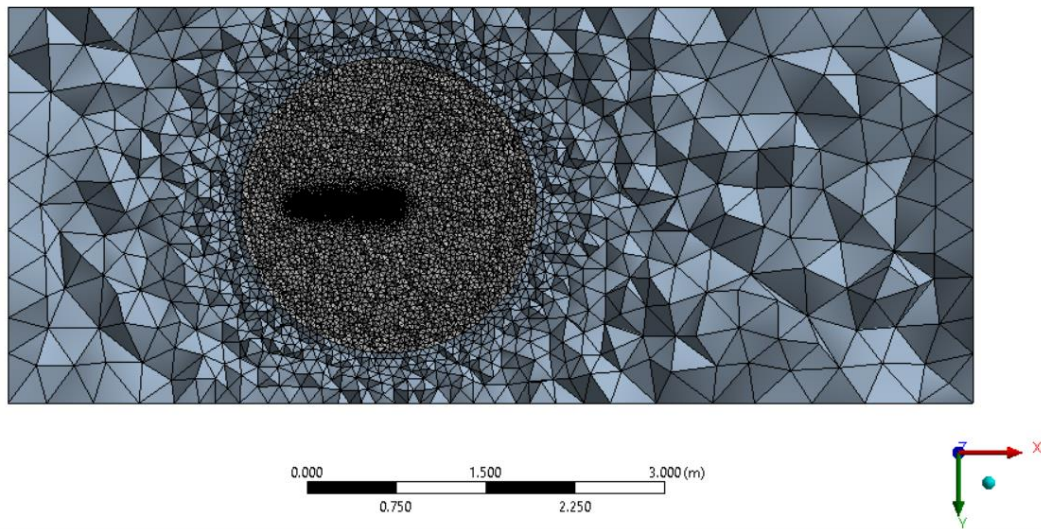


Figure 3.9 Mesh structure of the solution domain

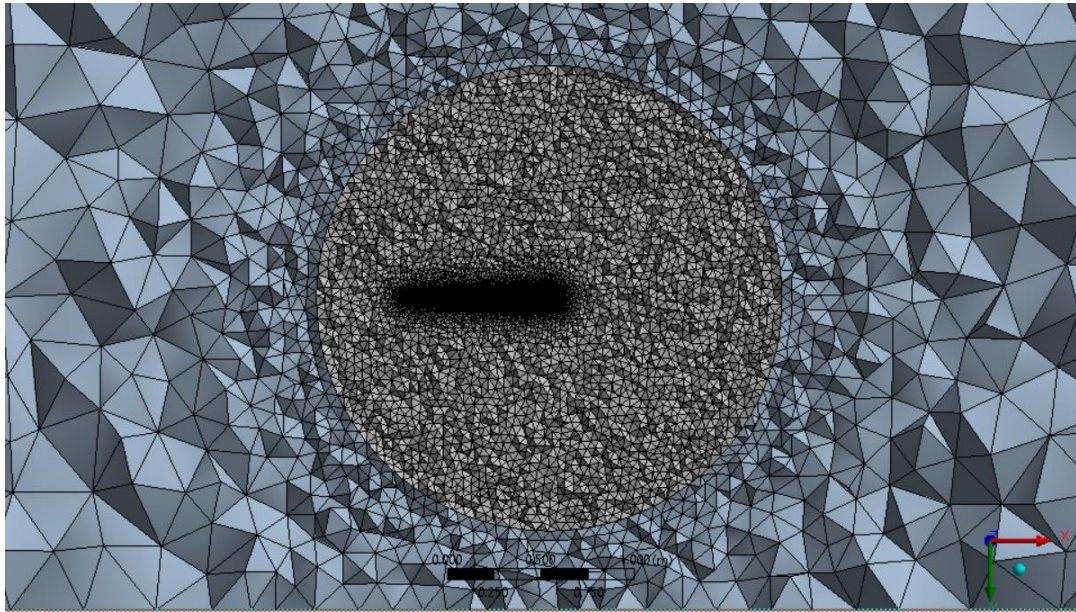


Figure 3.10 Cylinder body mesh structure

Mesh resolution inside the boundary layer around the arm is also important to consider, because pressure distribution on the arm and boundary layer separation affect the drag and lift forces. In accordance to the selected $k-\omega$ SST turbulence model, a wall resolved mesh with y^+ value around 1 is generated. For this purpose, a series of preliminary analyses for inflation layer using the straight arm model is made to capture y^+ to be less than or equal to 1, and it is assumed that the selected inflation layer parameters are also usable for the angled arm model. For these analyses, highest possible velocity values, which are 2 m/s for velocity inlet and 6.28 rad/s for rotational arm velocity, are selected, because if y^+ is around 1 for these values, then for slower velocities, y^+ should not exceed 1. Figure 3.11 shows y^+ values of the chosen inflation layers for different times during the hand/arm model's rotation. The results show that y^+ is less than or close to 1 at all times. Only the small portion of fingertip has around 1.3 y^+ value. Table 3.3 presents the details of the inflation layer mesh after y^+ analyses.

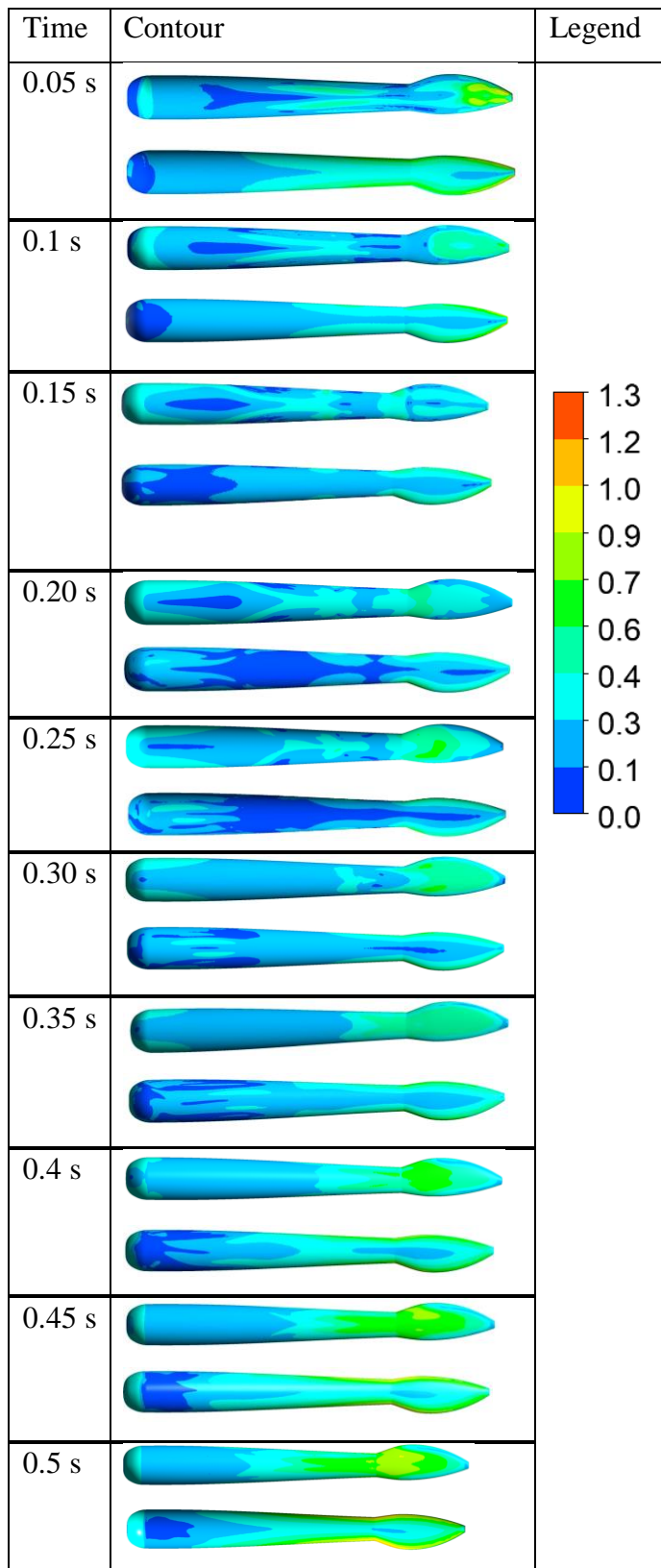


Figure 3.11 y^+ values on the arm at different times

Table 3.3 Details of the inflation (boundary layer) mesh

Inflation option	First layer thickness
First layer height	5e-6 m
Maximum layers	40
Growth rate	1.2
Maximum y+ values for mesh independence study for different times	0.6 ~1.2

Figure 3.12 shows the inflation layer mesh close to the shoulder. Figure 3.13 focuses on the mesh view close to the tip of the hand. Both figures shows that inflation layer captures the curvy surfaces of the arm.

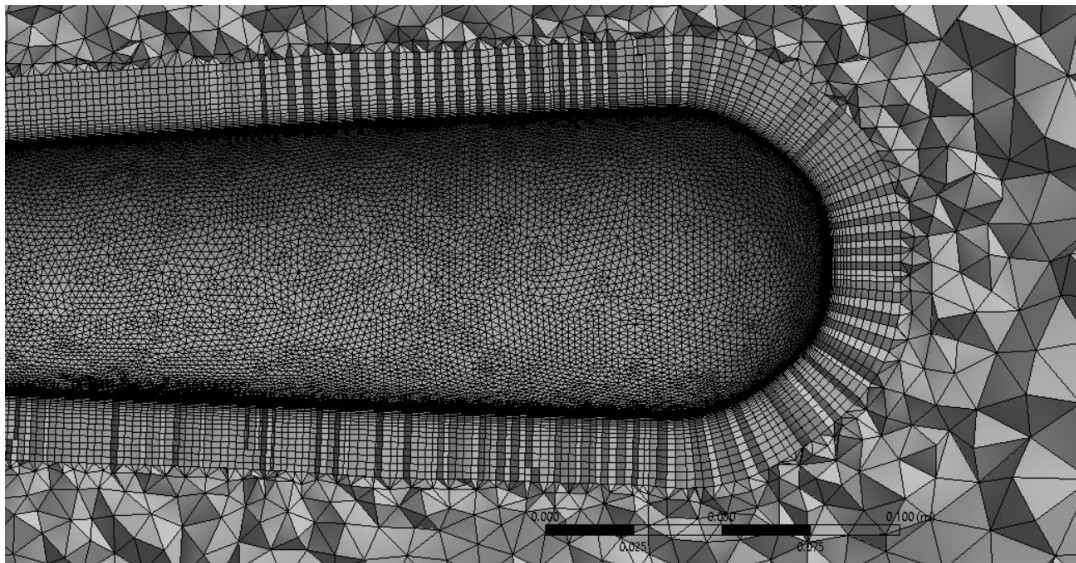


Figure 3.12 Inflation layer close to the shoulder

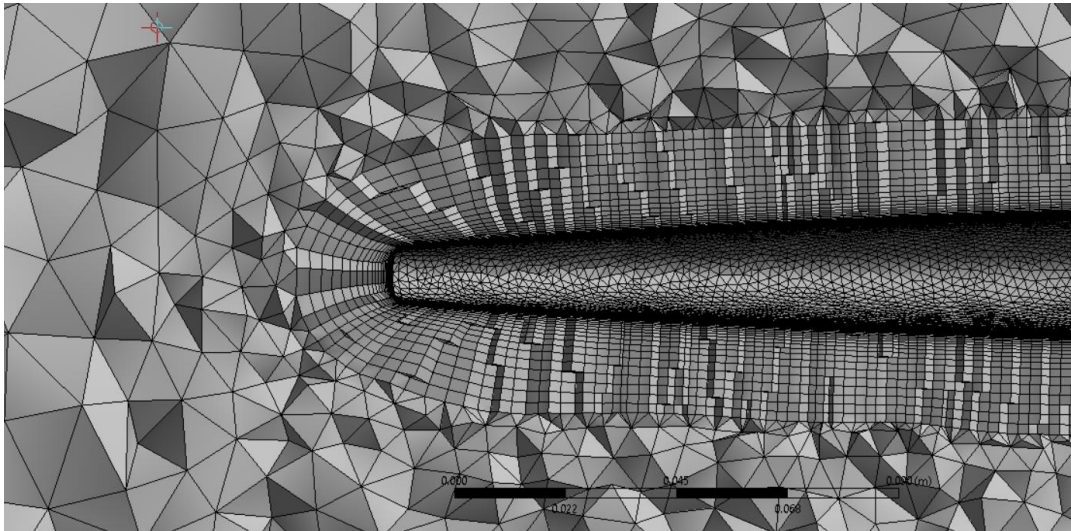


Figure 3.13 Inflation layer close to the tip of the hand

It is also important to obtain surface pressure results on hand/arm model, thus; creating fine mesh on hand/arm geometry is necessary. Figure 3.14 is a close view to the mesh structure on the hand segment.

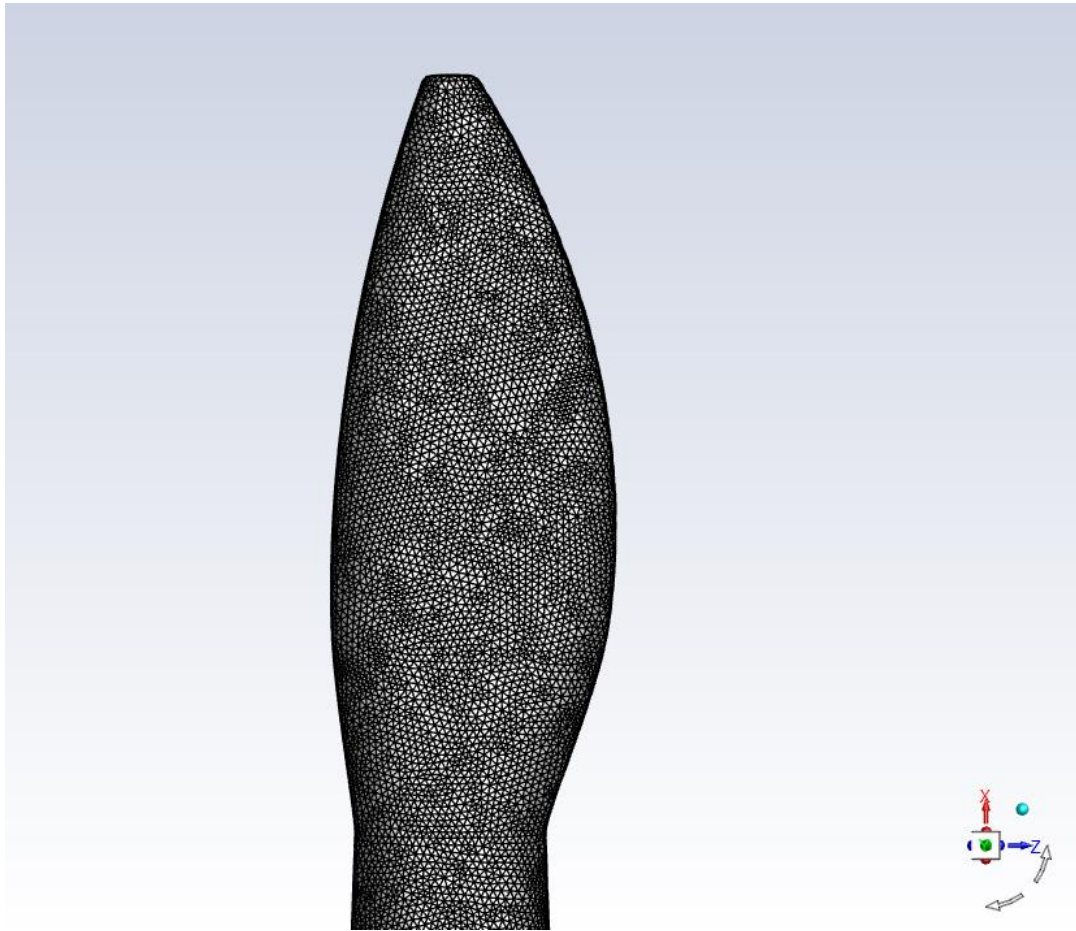


Figure 3.14 Mesh structure on hand segment

3.3.1 Mesh Independence Study

For CFD studies, it is important to make sure that the results are independent from the mesh resolution. For this purpose, a set of CFD analyses with systematically refined meshes is needed. This study is made until there is no significant change in the results by making the mesh finer. For the mesh independence study, highest inlet and rotational arm velocity values, i.e. 2 m/s and 6.28 rad/s, are selected, because these velocity values need the highest mesh resolution and the selected mesh from mesh independence study will be fine enough for other lower velocity values.

Table 3.4 shows the sizing parameters and values of the mesh independence study. This study starts with the coarsest mesh that accurately captures the curved geometrical details of the hand/arm model and this first mesh (Mesh-1 in Table 3.5) has approximately 340 thousand elements. Then, finer meshes are generated by gradually reducing values of the sizing parameters. Fig. 3.15 shows the result of the force acting on the arm in -x direction obtained with different meshes. Sweepback angle is the angle between flow direction and hand/arm direction. Main differences can be observed between 80° and 160°. The biggest difference can be seen between mesh-1 and mesh-2 around 140°. Other lines are relatively close to each other, yet there are still differences between mesh structures until between mesh-4 and mesh-5, which are very close to each other. Thus, from this mesh independence study, it is deduced that after mesh-4, which has around 4 million elements, results are independent from mesh resolution.

Table 3.4 Mesh independence study parameters. Mesh-4 is selected for the CFD analysis

All sizes are in m	MESH-1	MESH-2	MESH-3	MESH-4	MESH-5
Cylinder Sizing	0.3	0.08	0.07	0.05	0.03
Arm Sizing	0.008	0.006	0.0035	0.002	0.0015
Box Slope Sizing	0.2	0.09	0.08	0.07	0.06
Sliding Slope Sizing	0.2	0.09	0.08	0.07	0.06
Box Sizing	0.8	0.4	0.4	0.4	0.4
Hand Sizing	0.006	0.004	0.003	0.002	0.0015
Number of Elements	340K	710K	1.5M	4M	7.8M

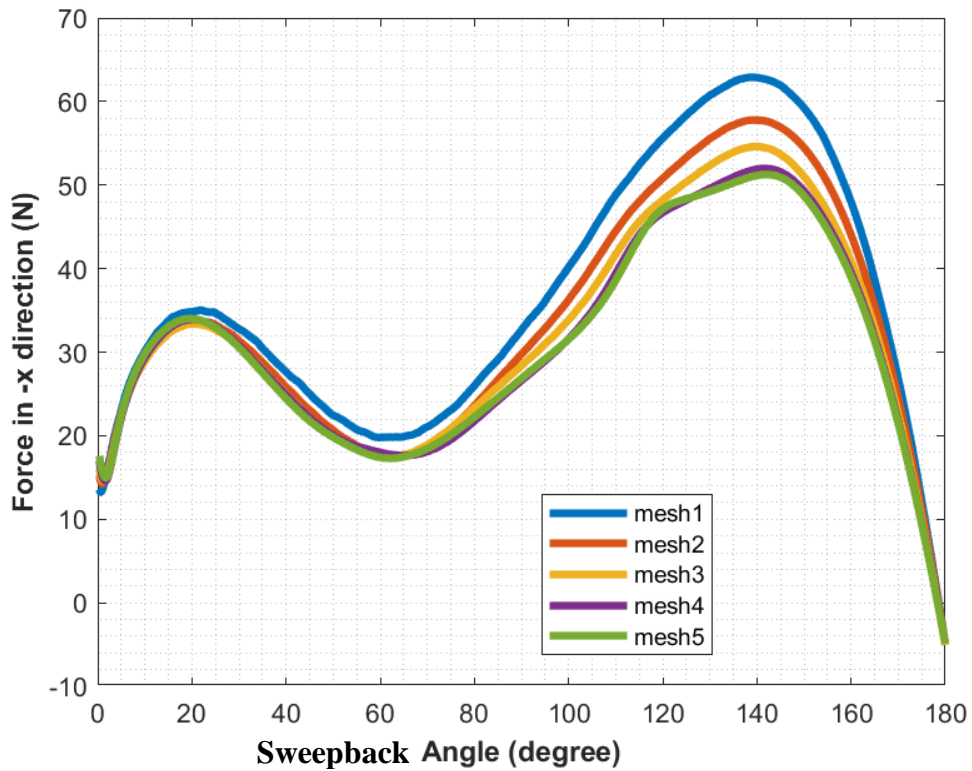


Figure 3.15 Force result in -x direction of the mesh independence study

3.3.2 Sliding Mesh Technique

Sliding mesh technique includes two or more cell zones that slide relative to each other using an interface surface without mesh deformation. Figure 3.16 shows the sliding mesh technique as used in this study. One cell zone, which is the cylinder region, rotates around its center and one cell zone remains stationary. Mesh interface helps two zones to make this rotation without deforming. In order to enable the sliding mesh technique, mesh motion is activated for the cylinder body in cell conditions inside ANSYS Fluent and rotational velocity is selected as 3.14 rad/s or 6.28 rad/s depending on the case.

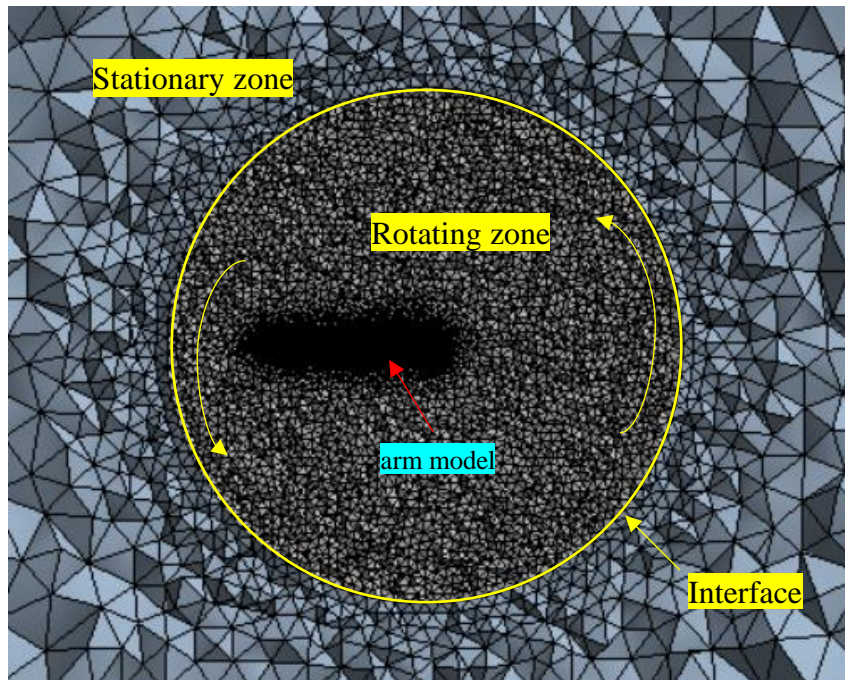


Figure 3.16 Sliding mesh technique for this study

3.4 CFD Setup

As mentioned in Section 3.2.1 and Table 3.1, there are 12 cases: six for the straight arm and six for the angled arm, and each analysis takes approximately 20 hours to complete with the available computational resources. Table 3.5 shows the CFD setup parameters. ANSYS Fluent software is used for all analyses. This study includes unsteady incompressible flow analysis thus, transient pressure-based solver type is selected. Turbulence model is chosen as $k-\omega$ SST. Water is the working fluid. Sliding mesh technique is used. Cylinder region's rotation around the z-axis in the counterclockwise direction is selected with speed of 3.14 rad/s or 6.28 rad/s, which depends on the investigated case. SIMPLE algorithm and first order upwind are used for discretization. The convergence criterion for the continuity equation is selected as 10^{-5} .

This study aims to compare straight arm and angled arm models during stroke. However, there are different rotational arm velocity values for some cases.

Therefore, number of time steps and time step size for unsteady flow analyses are chosen so that the arm model ends its rotation at 180° sweepback angle for all cases, which is assumed to be the end of the push phase of swimming. For this purpose, slower rotational arm velocity (3.14 rad/s) cases are divided into 800 time steps and time step size is selected as 0.00125 s, while faster rotational arm velocity (6.28 rad/s) cases have 1000 time steps and time step size is decided as 0.0005 s. For both cases, maximum iteration is chosen to be 35.

Table 3.5 CFD setup parameters

Setup	Option	
Software	ANSYS Fluent	
Solver Type	Pressure – Based, Transient	
Model	k- ω SST Turbulence Model	
Material	Water-liquid ($\rho = 1000 \frac{\text{kg}}{\text{m}^3}$, $\mu = 0.001 \text{ Pa} \cdot \text{s}$)	
Cell Zone Conditions	Cylinder rotation around z-axis in CCW direction, $\omega = 3.14 \text{ rad/s}$ or 6.28 rad/s	
Solution Method	SIMPLE, first order upwind	
Convergence Criteria	10^{-5} for continuity, 10^{-3} for others	
	Rotational Arm Velocity Cases (rad/s)	
	3.14	6.28
Number of Time Steps	800	1000
Time Step Size	0.00125 s	0.0005 s
Max iterations/ Time Step	35	35
Total Simulation Time	1 s	0.5 s

CHAPTER 4

RESULTS

After the CFD analysis is completed; observing and interpreting results such as velocity, pressure, and force in terms of fluid mechanics has an important place in understanding the effectiveness of arm strokes. Purposes of this study are to determine:

- Which arm model creates more propulsive force: Straight or elbow angled arm,
- At which sweepback angle the propulsive force is maximized,
- Which swimming case produces more propulsive force than others.

While doing this, it is also important to think about the factors that create and affect the propulsive force. For this purpose, this chapter first demonstrates the propulsive force results and then examines the pressure results in order to find its effect on propulsive force. Finally, velocity results are investigated in terms of low velocity and high velocity regions. Swimming cases are named in Table 3.1 for this chapter.

4.1 Propulsive Force Results

The force in the negative x-direction is defined as the propulsive force, as mentioned in Chapter 1. Figure 4.1 shows the variation of propulsive force with the sweepback angle for different swimming speed (in m/s) and rotational arm speed (in rad/s) cases. Solid lines are for the straight arm model, and dashed lines are for the angled models. In this work, from 0° to 20° sweepback angle zone is defined as entry/catch, from 20° to 90° zone is pull phase, from 90° to 160° is push phase and from 160° to 180° is defined as exit phase.

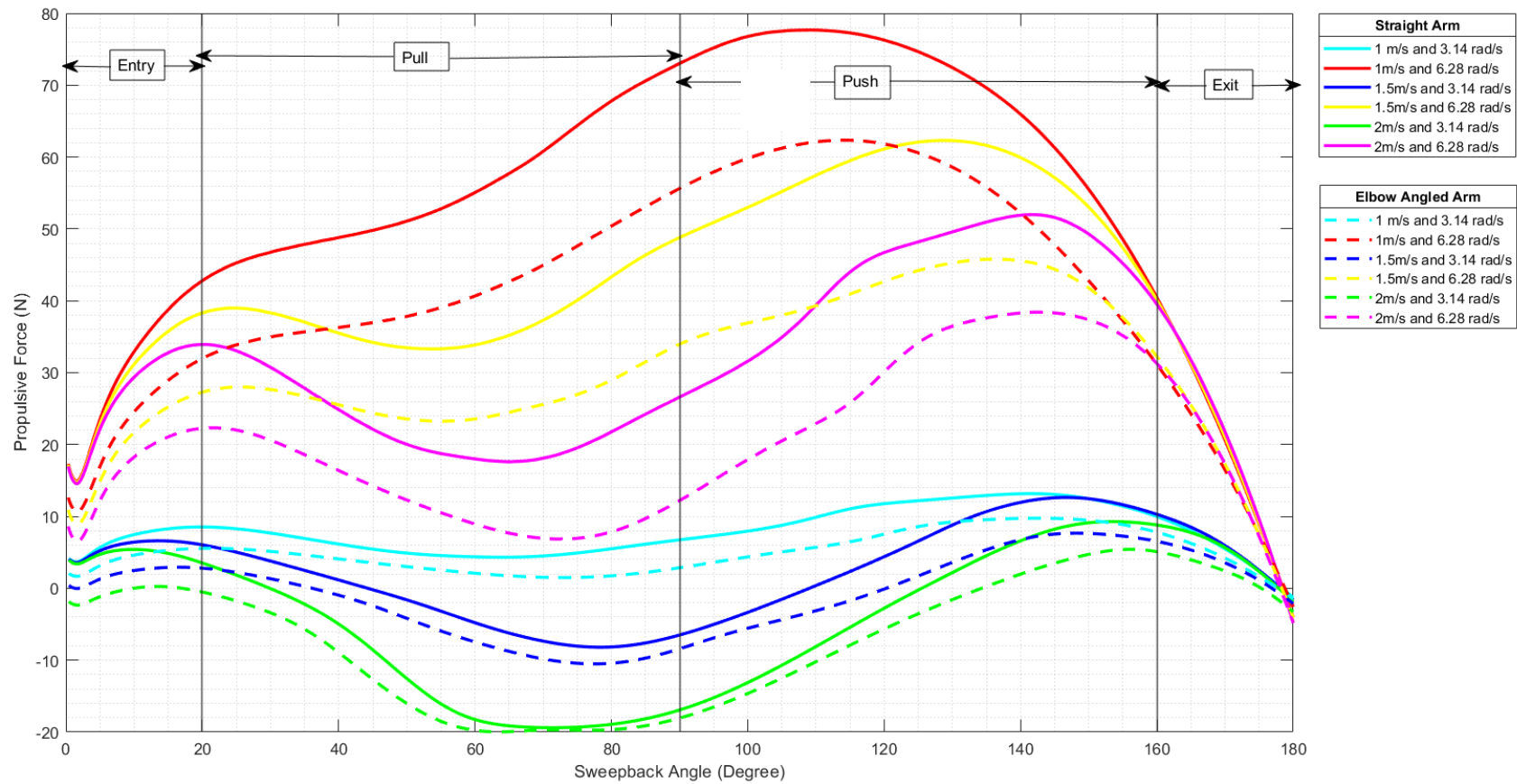


figure 4.1 Propulsive force values for different swimming cases at different sweepback angle

By observing the behavior of the solid lines, which are the straight arm cases, rotational arm speed of 6.28 rad/s creates more propulsive force than the 3.14 rad/s during the pull and push phases. This is also true for the angled models. This result is due to the fact that 6.28 rad/s creates larger stagnation pressure than 3.14 rad/s for the same surface area.

For every phase of the swimming, straight arm models create larger propulsive force than the corresponding angled ones. This is because when the arm is extended, meaning increasing length of the arm, the $\omega * R$ speed of the hand also increases. The faster the hand moves, the more propulsive force it produces. In swimming competitions, straight arm is more preferred for sprint phases (for short amounts of time due to increase of fatigue) in order to increase swimming velocity compared to the elbow angled case. Therefore, the propulsive force comparison between straight arm and elbow angled arm cases makes sense in this regard.

Between 12 swimming cases studied here, the highest propulsive force occurs for case 1B at every phase of swimming, except the exit phase. The lowest propulsive force is observed in the case 2E. As mentioned in Chapter 1 and illustrated in Fig. 1.10, moving forward creates drag force opposite to the propulsive force while arm rotation can produce normal force and its component may be in the same direction with propulsive force. Therefore, higher swimming speeds can lead to higher drag forces such that propulsive force can decrease. In a similar manner, higher rotational arm speed can increase propulsive force. Accordingly, it makes sense that the swimming case with the highest rotational arm speed and lowest swimming speed has the highest propulsive force produced. Likewise, the lowest propulsive force is seen for the highest swimming speed and the lowest rotational arm speed.

For 1.5 m/s & 3.14 rad/s, and 2 m/s & 3.14 rad/s cases, propulsive force becomes negative in pull and push phases for both straight and angled arms. This means that the net force is in the positive x-direction. In other words, drag force is dominant to the magnitude of normal force in swimming direction (see Fig. 1.10). Therefore, based on the models and the cases studied in this work, it can be concluded that if a

swimmer swims with a velocity of more than 1.5 m/s and would like to create propulsion in the swimming direction, he/she needs to rotate his/her arm with more than 3.14 rad/s. Compared to the other cases, propulsive force does not dramatically change throughout all swimming phases for the 1C and 2C cases. 1D, 2D, 1F, and 2F cases have decreasing propulsive force starting from the end of the entry phase to the middle of the pull phase and the same behavior is observed for 1C, 2C, 1E, and 2E. This means that at the beginning of the pull phase swimmers may need to rotate their arms faster in order to overcome this local drag force increase.

Locations of the maximum propulsive force differ slightly for different arm models and cases. For example, 1F reaches maximum propulsive force at the early part of the push phase, however the same case of the angled model reaches maximum propulsive force close to the middle part of the push phase. Table 4.1 shows the maximum propulsive force values and their locations in terms of sweepback angle. Among all swimming cases, maximum instantaneous propulsive force of 77.7 N at sweepback angle 109.4° is observed for case 1B (shown as grey highlight in Table 4.2). In addition, the rightmost column of Table 4.1 shows the maximum instantaneous propulsive force generated by each case as a percentage of this 77.7 N. As seen in this column, the lowest local maximum propulsive is only 7% of 77.7 N. One interesting result is that 1D and 2B have the same maximum propulsive force, which is 62.3 N, which occurs at 128.9° for the former and at 113.9° for the latter. Maximum propulsive force values for all cases are observed between 109.4° and 156.2° sweepback angles, which is similar with Sato and Hino's CFD study [23]. This means that maximum propulsive force occurs within the push phase.

Table 4.1 Observed maximum instantaneous propulsive force values and corresponding arm position in terms of sweepback angle.

Cases	Maximum Propulsive Force (N)	Sweepback Angle (Degree)	Normalized with respect to 77.7 N* (%)
1A	13.2	141.5	17.0
1B	77.7	109.4	100
1C	12.6	146.3	16.2
1D	62.3	128.9	80.2
1E	9.3	153.0	12.0
1F	52.0	141.5	66.9
2A	9.8	142.4	12.6
2B	62.3	113.9	80.2
2C	7.7	148.1	9.90
2D	45.8	136.1	59.0
2E	5.4	156.2	6.90
2F	38.4	142.9	43.6

* 77.7 N is the maximum propulsive force obtained among all cases.

Table 4.2 gives information about the mean propulsive force values for pull and push phases, where the most significant change in propulsive force occurs. Table 4.3 also includes total mean propulsive force values as well as created mean propulsive force by the hand and arm segments of the model. Highest mean propulsive force for the pull and push phases are 55.2 N and 68.1 N, respectively, both seen in the 1B. Rightmost column of Table 4.2 shows the difference of mean propulsive forces between pull and push phases. For all cases, mean propulsive force in the push phase is higher than the pull phase. Total mean propulsive force is 54.1 N and observed in 1B. For all cases, the hand segment creates more mean propulsive force than the arm segment, which is the same conclusion with Samson et al.'s study [21].

Table 4.2 Mean propulsive force during pull and push phases

Cases	Mean Propulsive Force		Hand	Arm	Total	Difference (Push-Pull) (N)
	Pull (N)	Push (N)				
1A	5.89	10.90	13.34	2.34	7.84	5.01
1B	55.19	68.07	75.18	32.97	54.07	12.88
1C	-2.30	5.46	9.57	-4.94	2.31	7.76
1D	37.93	55.58	63.94	20.08	42.01	17.65
1E	-11.24	-1.05	5.6	-13.65	-4.02	10.19
1F	23.63	43.14	52.98	9.37	31.18	19.51
2A	3.16	7.39	10.12	-0.18	4.97	4.23
2B	41.07	53.82	61.67	21.50	41.59	12.75
2C	-4.76	1.42	6.82	-8.58	-0.88	6.18
2D	26.52	40.55	50.76	9.66	30.21	14.03
2E	-13.55	-4.18	3.59	-17.61	-7.01	9.37
2F	13.09	29.47	40.22	-0.14	20.04	16.38

4.2 Pressure Results

Figure 4.2 shows the mean pressure differences between anterior and posterior parts of the hand/arm models at different sweepback angles. For this figure, data at 10 sweepback angles from 20° to 180° are used (data for the entry phase was not collected due to having non-physical results at $\theta = 0^\circ$). Color codes of the curves used are the same as with Fig 4.1. The solid curve indicates the straight arm and the dashed curve indicates the elbow angled arm. Grey vertical curves separate swimming phases: pull, push, and exit.

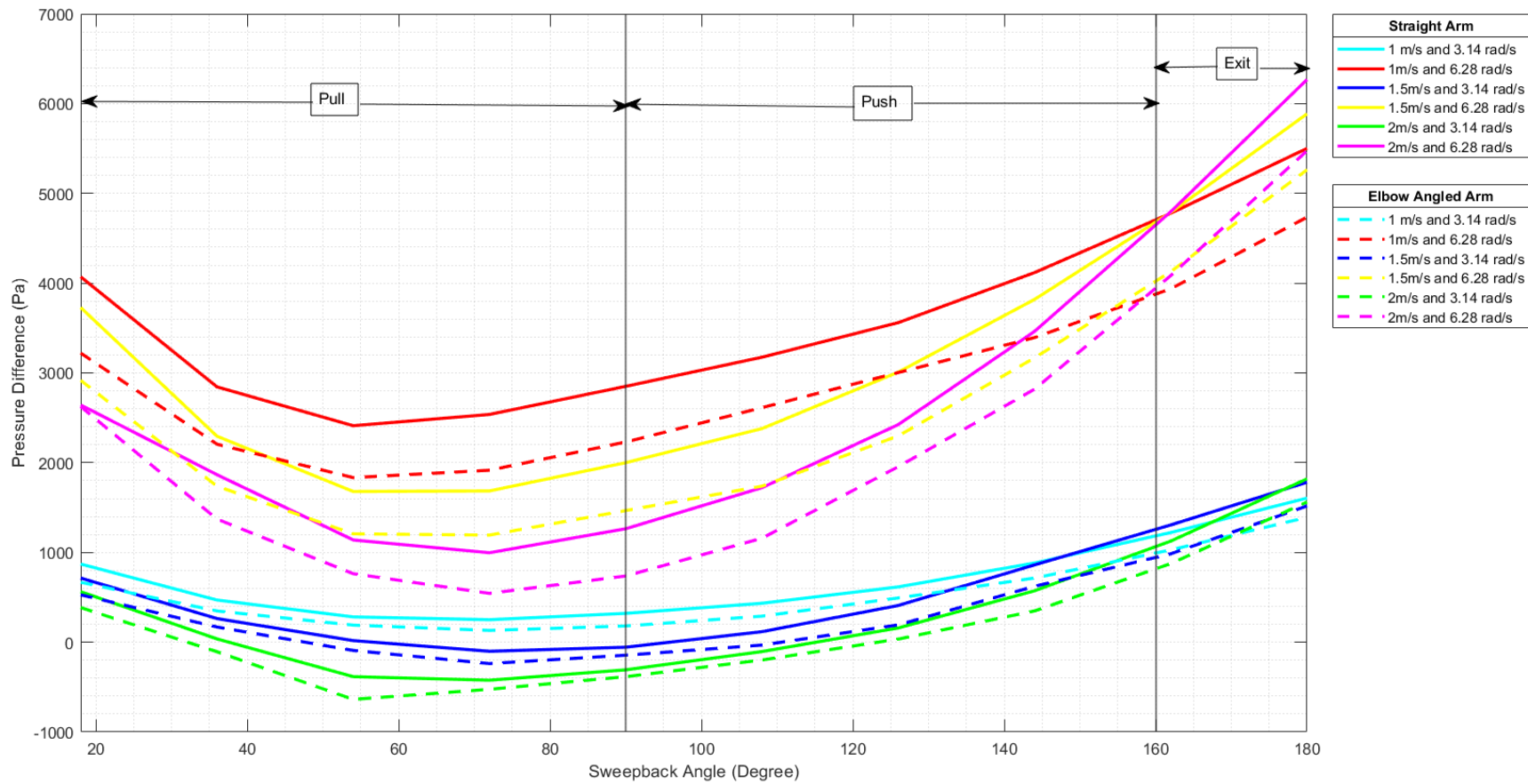


Figure 4.2 Mean Pressure Differences between Anterior and Posterior part of the Hand/Arm

Throughout the pull and push phases, 1B has the highest pressure difference. For the same swimming case, the straight arm model has higher pressure differences than the angled arm model. All of the 6.28 rad/s cases have higher pressure difference than the 3.14 rad/s cases. All these results are also parallel to what was observed in Fig. 4.1, showing that the mean pressure differences on the models are the main cause of the generated propulsive forces. In exit phase, 1F has the highest and 1D has the second highest pressure difference. This means that a higher swimming velocity leads to a higher pressure difference in the exit phase. However, this high pressure difference does not lead to higher propulsive forces than the 1B case, because of the orientation of the arm in the exit phase and how most of the pressure imbalance contributes to lift, rather than propulsion. Highest pressure differences are also observed in Sato and Hino's study [23]

Figure 4.3 shows high and low pressure regions in the x-y plane ($z=0$) of 1B and 2B, which are the cases that produce highest propulsive forces, for different sweepback angles. For better comparison, same view of different sweepback angle positions are selected. Red and blue colors show the regions that have pressures higher than 1014 Pa, and pressures lower than -3420 Pa, respectively. In all sweepback angles, high pressure region occurs around the palm for both models. Anterior part of the forearm, close to the wrist also experiences high pressure, however, this is not as dominant as the palm. For the straight arm, high pressure region reaches the elbow level at the beginning of the pull phase. Then, the region starts shrinking to the middle part of the forearm anterior until the end of the pull phase, which is sweep angle $\theta = 90^\circ$. Then, it again expands along the forearm and reaches the elbow level at $\theta = 144^\circ$. After this angle, or at push phase, high pressure zone reaches to a limited part of upper arm anterior level. Same behavior can be seen for the angled case. Low pressure region mostly occurs at the back side of the hand and the posterior part of the forearm. At first two θ values, low pressure regions expand to the tip of the hand. However, for the rest of the simulation, low pressure region occurs around the wrist (some region is around the back of the hand and a limited region is around forearm posterior). Similar to the high pressure region, low pressure region is more dominant

around the hand than the forearm. For all sweepback angles, high and low pressure areas in the straight arm case are greater than the elbow angled arm case. The largest high and low pressure regions and their differences occur at $\theta=180^\circ$ for both straight and elbow angled arm.

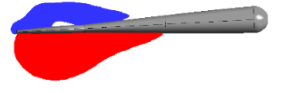
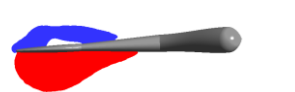
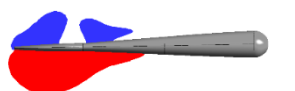
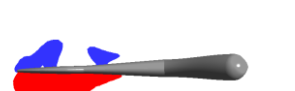


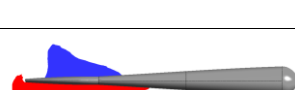

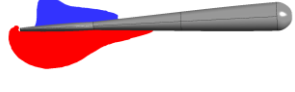


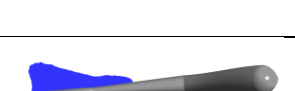
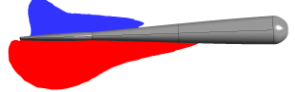
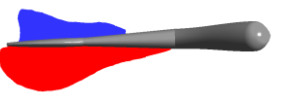


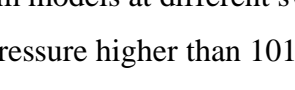
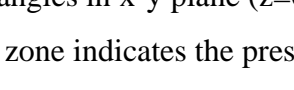


Sweep. Ang. (θ)	Straight Arm	Angled Arm
18°		
36°		
54°		
72°		
90°		
108°		
126°		
144°		
162°		
180°		

Figure 4.3 High and low pressure regions around 1 m/s & 6.28 rad/s case of the straight and angled arm models at different sweepback angles in x-y plane ($z=0$). Red zone shows the pressure higher than 1014 Pa; blue zone indicates the pressure is lower than -3420 Pa.

4.3 Velocity Results

Figure 4.4 shows the speed contours obtained using velocity vectors relative to the rotating cylindrical region that includes the arm (see Fig. 3.9). The cases selected for this figure are the one that produce the highest propulsive force, i.e. 1B, and the one that produces the lowest propulsive force, i.e. 2E. Contours of highest propulsive force swimming case (1B) are located on the left and the lowest (2E) is on the right. There are ten sweepback angles investigated. The dominant color of the straight arm, which is blue, indicates the swimming velocity of 1m/s, which is turquoise for the angled model, indicating 2m/s. For the straight arm model velocity contour at $\theta = 18^\circ$, a stagnation is observed at the fingertip, and starting from back of the hand, flow accelerates up to 7.6 m/s by generating a flow region which surpasses 1.5 m/s. A low velocity region can be observed at the shoulder. A small, accelerated flow region also occurs around the palm and forearm anterior, however this region is not as large. From $\theta = 36^\circ$ to 72° , the accelerated flow region is enlarged, yet the flow slows down compared to 18° . Starting from 90° , higher velocities can be observed inside the accelerated flow region, and this zone expands for the rest of the simulation. Starting from 108° , accelerated flow region keeps expanding and creates a concave region. On the other hand, angled arm model does not have an accelerated flow region as dominant as the straight model. Since the speed contours are shown on the x-y plane ($z=0$) in this figure, the details around the upper arm and the shoulder cannot be seen for the angled model. However, there is no significant speed variation in this region anyway. At 18° , accelerated flow region occurs, similar to the straight arm case, but the region is smaller and has lower speed values. For 36° , accelerated flow region is larger than the case at 18° , with lower speeds. For all sweepback angles, keeping in mind that the velocities for the two cases are different, it can still be observed that the angled arm model does not have a strong accelerated region as seen for the straight arm case. Therefore, it can be deduced that in order to create a propulsive force (for 2E, propulsive force becomes negative in some sweepback angles), swimmers should rotate their arms faster than the swimming velocity so that

they create an accelerated flow region as seen in the 1B. This accelerated flow region close to hand is the reason for low pressure, and propulsive force generation.

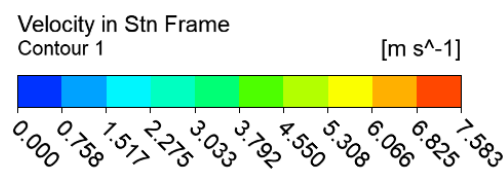
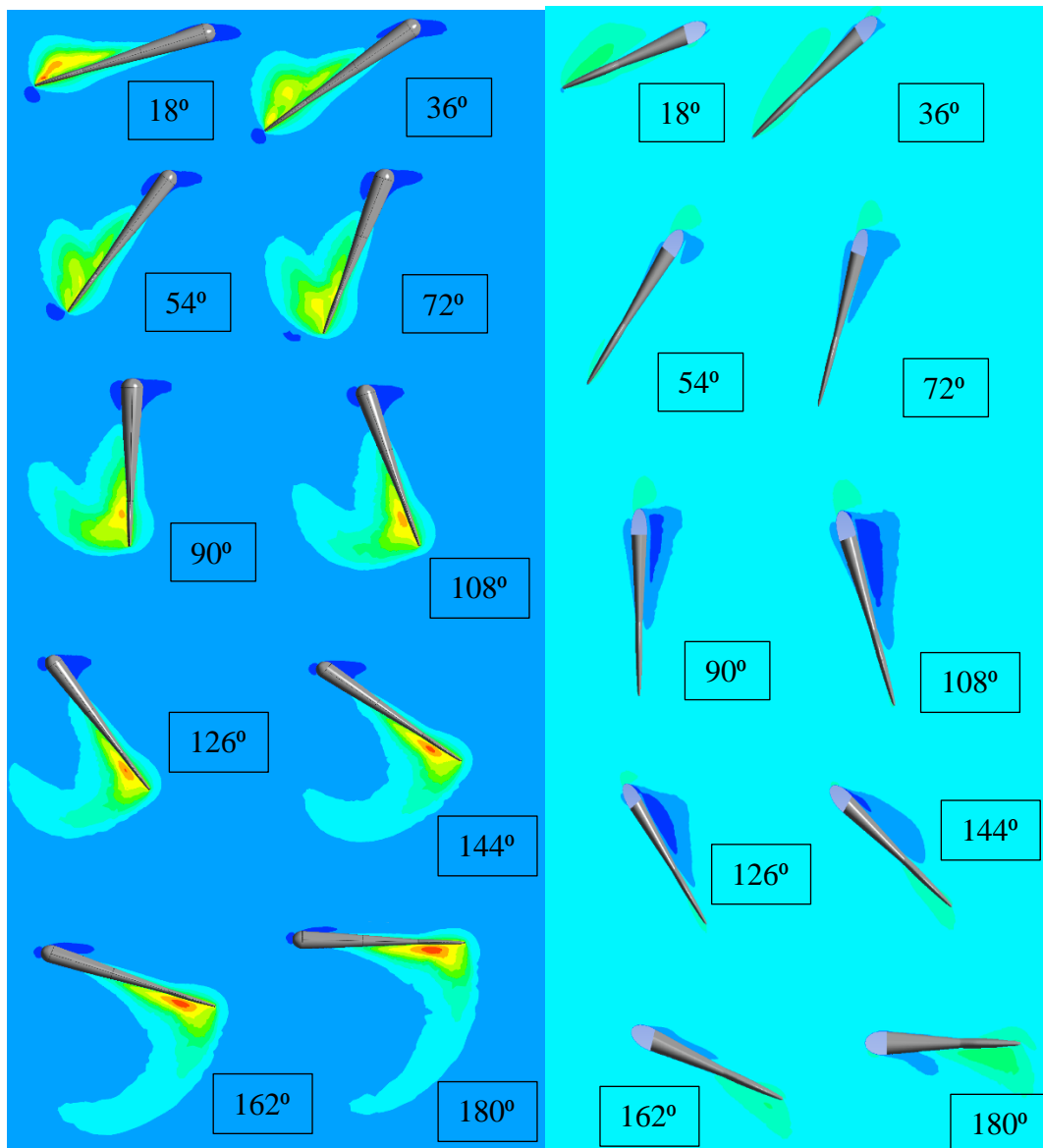


Figure 4.4 Relative velocity (with respect to the cylinder body) contour of the swimming case that has highest propulsive force. Contour on the left belongs to 1B which is highest propulsive force observed case and, on the right, belongs to 2E, which is the lowest. Sweepback angle values of the hand/arm positions are located on the right-lower side of the each hand/arm model.

CHAPTER 5

CONCLUSION

5.1 Summary of the Study

Most research on fluid mechanics focuses on the reduction of negative effects of the fluid environment, such as drag. Swimming is one of the fascinating areas that benefits from the fluid environment. In swimming, swimmers move their limbs in order to create the propulsive force that is needed to move forward. Hand/arm segment is the dominant limb during swimming strokes. Thus, it is important to understand how hand/arm segment creates the propulsive force. However, muscular effort, which has an important role in creating propulsive force is not considered in this study. In swimming, there are also different phases when swimmers must swim faster or save their energies for later on. Therefore, it is also crucial to identify which phase results in greater propulsive force than others.

This study investigates 12 swimming cases for two arm models used in front crawl swimming by using unsteady 3D CFD analysis in ANSYS Fluent. For this purpose, a straight arm model that is mostly used for sprint swimming and 145° elbow angled arm, which is preferred in middle or long distance front crawl swimming, are created in ANSYS Spaceclaim. k- ω SST turbulence model is chosen for the CFD analysis. An optimal mesh is found using a mesh independence study by using the parameters of the fastest swimming velocity and rotational arm velocity case of straight arm which are 2m/s and 6.28rad/s. The selected mesh has 4M elements. For the analysis, sliding mesh technique is used to obtain rotational arm velocity. 1, 1.5 and 2 m/s, which are commonly observed velocities in swimming are selected as inlet velocities and 3.14 rad/s and 6.28 rad/s are chosen as rotational arm velocities to ensure that after one stroke, the arm rotates 180° and reaches the exit phase of front crawl

swimming. For this purpose, for 3.14 rad/s, simulation time is selected as 1s and for 6.28 rad/s simulation time is selected 0.5s to reach 180° sweepback angle for both cases.

5.2 Major Conclusions

In light of the models and the results presented in this thesis, some major conclusions may be summarized as follows.

- 1 m/s and 6.28 rad/s swimming case has the highest propulsive force, 2 m/s and 3.14 rad/s has the lowest propulsive force. Thus, swimmers should rotate their arms faster than the swimming velocity in order to get good amount of propulsive force.
- Straight arm model creates 1.5 times higher propulsive force than elbow angled arm on average. Thus, swimmers who need to create propulsive force should keep their arm as straight as possible.
- Push phase creates more propulsive force than pull phase in all cases. $\theta=110^\circ$ to 150° are important to create more propulsive force. This result is similar with what Sato and Hino's study [23] found. Therefore, swimmers may try saving their energies for push phase.
- The hand segment creates more propulsive force than the arm segment. This result was also observed in Samson et al.'s study [21].

5.3 Future Work

The model of this study has some deficiencies due to not having sufficient computational resources. In addition, the time duration was limited for simulating more complex swimming motions and modeling more realistic flow conditions. After this study, making experimental studies with a human subject and adding complex motions to the problem are suggested for further studies. Some of the possible future works are listed below:

- Not only the hand and arm but also the other parts of body could be added for further analysis to better mimic realistic swimming motions.
- Gravitational effects could be considered.
- Complex arm motions rather than only rotational motion could be considered to increase the reality of swimming motion in CFD analysis.
- Rather than constant velocity, acceleration could also be investigated to understand different swimming paces.
- Free surface condition between air and water phases can be added to the model.

REFERENCES

- [1] H. V. Dijk, R. V. Meegen and G. Vroemen, *The secret of cycling: maximum performance gains through effective power metering and training analysis*, Meyer & Meyer Sport, 2017.
- [2] R. E. Schleihauf, "A hydrodynamic analysis of swimming propulsion," *Swimming III. Proceedings of the Third International Symposium of Biomechanics in Swimming, University of Alberta, Edmonton, Canada*, pp. 70-109, 1979.
- [3] H. Takagi and R. Sanders, "Measurement of propulsion by the hand during competitive swimming," *The Engineering of Sport*, vol. 4, pp. 631-637, 2002.
- [4] M. A. Berger, G. de Groot and A. P. Hollander, "Hydrodynamic drag and lift forces on human hand/arm models," *Journal of biomechanics*, vol. 28, no. 2, pp. 125-133, 1995.
- [5] R. Sanders, "Hydrodynamic characteristics of a swimmer's hand," *Journal of Applied Biomechanics*, vol. 15, pp. 3-26, 1999.
- [6] H. Takagi, Y. Shimizu, A. Kurashima and R. Sanders, "Effect of thumb abduction and adduction on hydrodynamic characteristics of a model of the human hand," in *Proceedings of Swim Sessions of the XIX International Symposium on Biomechanics in Sports*, San Francisco: University of San Francisco, 2001.
- [7] P. Gardano and P. Dabnichki, "On hydrodynamics of drag and lift of the human arm," *Journal of Biomechanics*, vol. 39, pp. 2767-2773, 2006.
- [8] J. Tu, G.-H. Yeoh and C. Liu, *Computational Fluid Dynamics: A Practical Approach*, Butterworth-Heinemann, Elsevier Publication, 2018.

- [9] S. Taormina, *Swim speed strokes for swimmers and triathletes: Master Butterfly, backstroke, breaststroke, and freestyle for your fastest swimming*, Boulder, CO: VeloPress, 2014.
- [10] "Dick's Pro Tips," [Online]. Available: <https://protips.dickssportinggoods.com/sports-and-activities/water-sports/how-to-improve-your-freestyle-stroke-in-five-steps>. [Accessed 28 09 2021].
- [11] P. Newsome and A. Young, *Swim Smooth: The complete coaching programme for swimmers and triathletes*, John Wiley & Sons, 2012.
- [12] B. Bixler and S. Riewald, "Analysis of a swimmer's hand and arm in steady flow conditions using computational fluid dynamics.," *Journal of Biomechanics*, vol. 35, no. 5, pp. 713-717, 2002.
- [13] A. Rouboa, A. Silva, L. Leal, J. Rocha and F. Alves, "The effect of swimmers hand/forearm acceleration on propulsive forces generation using computational fluid dynamics," *Journal of Biomechanics*, vol. 39, no. 7, pp. 1239-1248, 2006.
- [14] D. A. Marinho, A. Rouboa, A. Silva, J. P. Vilas-Boas, F. B. Alves, L. Machado and V. M. Reis, "The use of Computational Fluid Dynamics in swimming research," *International Journal for Computational Vision and Biomechanics*, vol. 3, no. 1, pp. 13-16, 2017.
- [15] B. S. Rushall, E. J. Sprigings, L. E. Holt and J. M. Cappaert, "A re-evaluation of forces in swimming., 10, 6-30.," *Journal of Swimming Research*, vol. 10, pp. 6-30, 1994.
- [16] N. O. Sidelnik and B. W. Young, "Optimising the freestyle swimming stroke: The effect of finger spread," *Sports Engineering*, vol. 9, no. 3, pp. 129-135, 2006.

- [17] H. Takagi, M. Nakashima, T. Ozaki and K. Matsuuchi, "Unsteady hydrodynamic forces acting on a robotic arm and its flow field: application to the crawl stroke," *Journal of biomechanics*, vol. 47, no. 6, p. 1401–1408, 2014.
- [18] M. Samson, T. Monnet, A. Bernard, P. Lacouture and L. David, "Kinematic hand parameters in front crawl at different paces of swimming," *Journal of Biomechanics*, vol. 48, no. 14, pp. 3743-3750, 2015.
- [19] V. Gourgoulis, A. Boli, N. Aggeloussis, P. Antoniou, A. Toubekis and G. Mavromatis, "The influence of the hand's acceleration and the relative contribution of drag and lift forces in front crawl swimming," *Journal of Sports Sciences*, vol. 33, no. 7, pp. 696-712, 2014.
- [20] M. Bilinauskaite, V. R. Mantha, A. I. Rouboa, Z. P. and A. J. & Silva, "A Computational Fluid Dynamics Study of Propulsion Due to the Orientation Effects of Swimmer's Hand," *Journal of Applied Biomechanics*, vol. 29, no. 6, pp. 817-823, 2013.
- [21] M. Samson, A. Bernard, T. Monnet, P. Lacouture and L. David, "Unsteady computational fluid dynamics in front crawl swimming," *Computer methods in biomechanics and biomedical engineering*, vol. 20, no. 7, pp. 783-793, 2017.
- [22] G. Lecrivain, A. Slaouti, C. Payton and I. Kennedy, "Using reverse engineering and computational fluid dynamics to investigate a lower arm amputee swimmer's performance," *Journal of Biomechanics*, vol. 41, no. 13, pp. 2855-2859, 2008.
- [23] Y. Sato and T. Hino, "A Computational Fluid Dynamics Analysis of Hydrodynamic Force Acting on a Swimmer's Hand in a Swimming

- Competition," *Journal of Sports Science and Medicine*, vol. 12, pp. 679-698, 2013.
- [24] S. Kudo, R. Vennell and B. Wilson, "The effect of unsteady flow due to acceleration on hydrodynamic forces," *Journal of Biomechanics*, vol. 46, pp. 1697-1704, 2013.
- [25] R. C. Z. Cohen, P. W. Cleary, B. R. Mason and D. L. Pease, "Forces during front crawl swimming at different stroke rates," *Sports Engineering*, vol. 21, no. 1, pp. 63-73, 2017.
- [26] P. Dabnichki, "Unsteady fluid mechanics effects in water based human locomotion," *Mathematics and Computers in Simulation*, vol. 82, no. 3, pp. 471-482, 2011.
- [27] R. Bazuin, "The effects of hand configuration on propulsive forces in swimming (thesis).," 3 May 2018. [Online]. Available: <http://resolver.tudelft.nl/uuid:6e704a41-64d2-4601-9355-4f506e23bc6a> .
- [28] J. van Houwelingen, D. H. J. Willemsen, R. P. J. Kunnen, G. F. van Heijst, E. J. Grift, W. P. Breugem, R. Delfos, J. Westerweel, H. J. H. Clercx and W. van de Water, "The effect of finger spreading on drag of the hand in human swimming," *Journal of Biomechanics*, vol. 63, pp. 67-73, 2017.
- [29] L. E. Gomes and J. F. Loss, "Effects of unsteady conditions on propulsion generated by the hand's motion in swimming: a systematic review," *Journal of Sports Sciences*, 2015.
- [30] ANSYS, ANSYS Fluent Theory Guide, Canonsburg, PA, 2013.
- [31] G. Singha, A. Singlaa and G. S. Virkb, "Modeling and Simulation of a Passive Lower-Body Mechanism for Rehabilitation," in *Conference on*

Mechanical Engineering and Technology (COMET-2016), Department of Mechanical Engineering, IIT (BHU), Varanasi, 2016.

- [32] S. Adewusi, M. Thomas, V. H. Vu and W. Li, "Modal parameters of the human hand-arm using finite element," *Mechanics & Industry*, vol. 15, pp. 541-549, 2014.